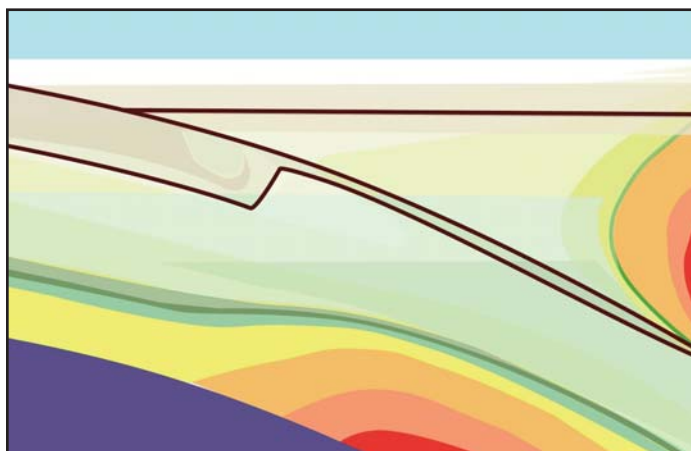# ANDREW HYNES SERIES: TECTONIC PROCESSES

Geologic Setting of Eclogite-facies Assemblages in the St. Cyr Klippe, Yukon–Tanana Terrane, Yukon, Canada

M.B. Petrie[1], J.A. Gilotti[1], W.C. McClelland[1], C. van Staal[2], and S.J. Isard[1]

[1]*Department of Earth and Environmental Sciences
University of Iowa, Iowa City, Iowa 52242, USA
E-mail: mbpetrie@gmail.com*

[2]*Natural Resources Canada
Geological Survey of Canada
Vancouver, British Columbia, V6B 5J3, Canada*

SUMMARY

The St. Cyr area near Quiet Lake hosts well-preserved to variably retrogressed eclogite found as sub-metre to hundreds of metre-long lenses within quartzofeldspathic schist in south-central Yukon, Canada. The St. Cyr klippe consists of structurally imbricated, polydeformed and polymetamorphosed units of continental arc crust and ultramafic–mafic rocks. Eclogite-bearing quartzofeldspathic schist forms thrust slices in a 30 km long by 6 km wide, northwest-striking outcrop belt. The schist unit comprises metasedimentary and felsic intrusive rocks that are intercalated on the metre to tens of metres scale. Ultramafic rocks, serpentinite and associated greenschist-facies metagabbro form imbricated tectonic slices within the eclogite-bearing quartzofeldspathic unit, which led to a previously held hypothesis that eclogite was exhumed within a tectonic mélange. The presence of phengite and Permian zircon crystallized under eclogite-facies metamorphic conditions in the quartzofeldspathic host rocks indicate that the eclogite was metamorphosed *in situ* together with the schist as a coherent unit that was part of the continental arc crust of the Yukon–Tanana terrane, rather than a mélange associated with the subduction of oceanic crust of the Slide Mountain terrane. Petrological, geochemical, geochronological and structural similarities link St. Cyr eclogite to other high-pressure localities within Yukon, indicating the high-pressure assemblages form a larger lithotectonic unit within the Yukon–Tanana terrane.

RÉSUMÉ

La région de St-Cyr renferme des éclogites bien conservées à légèrement rétrogradées qui se présentent sous forme de lentilles allant de la fraction de mètre à quelques centaines de mètres de longueur, au sein d'un schiste quartzofeldspathique du centre-sud du Yukon au Canada. La klippe de St-Cyr est structurellement constituée d'unités imbriquées, polydéformées et polymétamorphisées de croûte d'arc continental et de roches ultramafiques à mafiques. Les schistes quartzofeldspathiques à lentilles d'éclogites forment des écailles de chevauchement d'une bande de 30 km de longueur par 6 km de largeur de direction nord-ouest. Les schistes sont constitués de roches métasédimentaires et de roches intrusives felsiques intercalées à des intervalles qui vont du mètre à quelques dizaines de mètres. Les roches ultramafiques, serpentinites et métagabbros au facies à schiste vert forment des écailles tectoniques imbriquées au sein de l'unité quartzofeldspathique à lentilles d'éclogite, d'où une précédente hypothèse voulant que les éclogites soient un produit d'exhumation à partir d'un mélange tectonique. La présence de phengite et de zircon permien cristallisé sous conditions métamorphiques du faciès à éclogite au sein de la roche hôte quartzofeldspathique indiquent que l'éclogite a été métamorphisée en place, avec le schiste comme unité cohérente du terrane de croûte d'arc continental de Yukon–Tanana, plutôt qu'un mélange associé à une subduction de croûte océanique du terrane de Slide Mountain. Des similarités pétrologiques, géochimiques, géochronologiques et structurales lient les éclogites de St-Cyr à d'autres lieux de hautes pressions au Yukon, ce qui indique que les
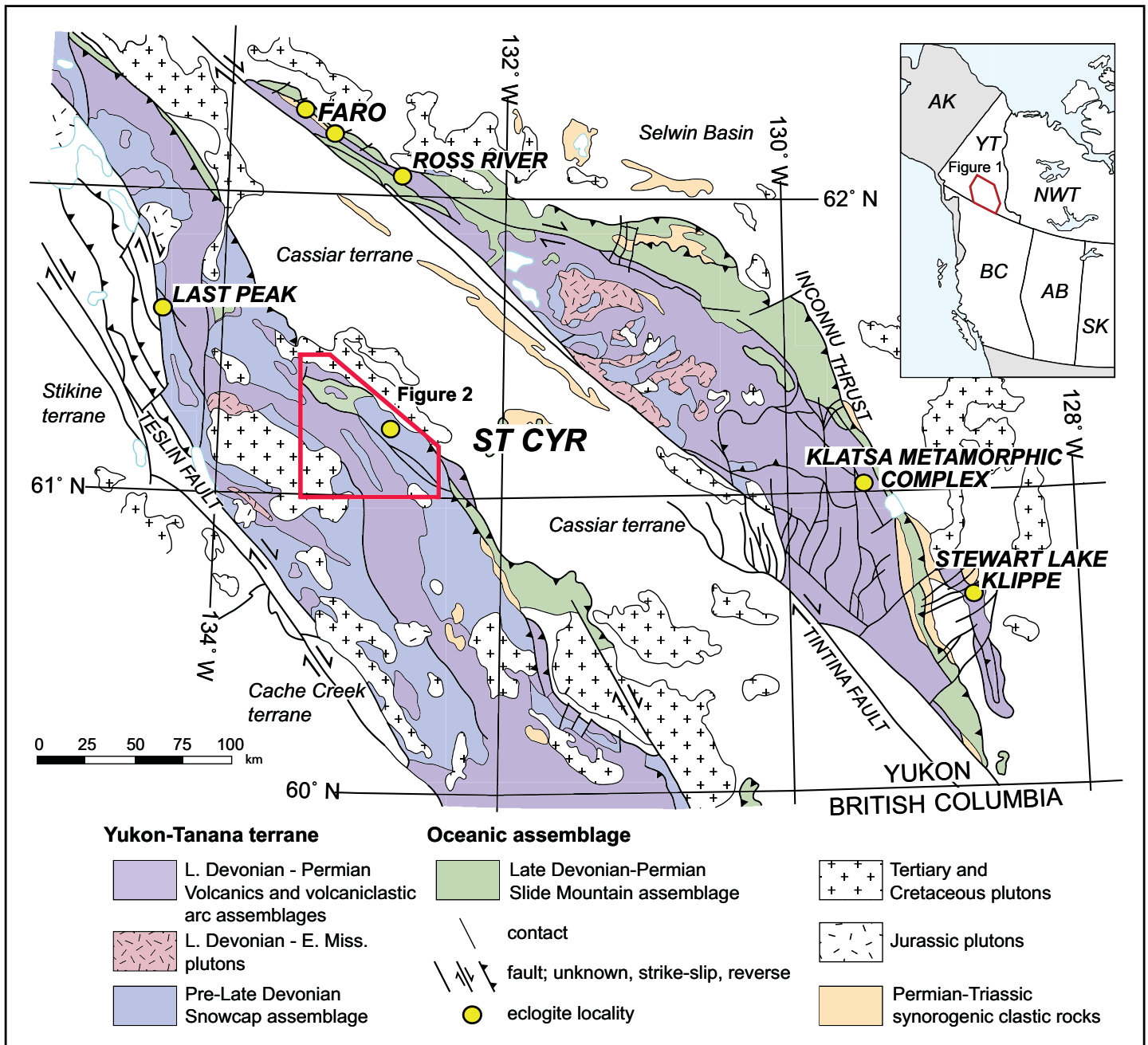
Figure 1. Regional geologic map of the Yukon-Tanana and Slide Mountain terranes in south-central Yukon (modified from Colpron et al. 2006a).

assemblages de hautes pressions forment une unité lithotectonique plus grande au sein du terrane de Yukon–Tanana.

INTRODUCTION

High-pressure metamorphic assemblages formed in Pacific-type convergent margins, such as the iconic Franciscan complex (Ernst 2015), are found along the western North American margin from Alaska to Mexico (Erdmer et al. 1998). The Yukon–Tanana terrane in the Canadian Cordillera preserves both Mississippian and Permian high-pressure rocks. In southeastern Yukon (Fig. 1), strongly retrogressed, Early Mississippian eclogite-facies rocks are preserved as pods within a tectonic mélange in the Klatsa metamorphic complex (Devine et al. 2006), the Simpson Range (Creaser et al. 1999) and the

Stewart Lake klippe (Erdmer 1987; Erdmer et al. 1998). These high-pressure rocks are inferred to have formed during east-directed subduction of Panthalassa beneath the western edge of the Yukon–Tanana arc and then were transported eastward in Mesozoic thrust sheets (Erdmer et al. 1998; Devine et al. 2006). In contrast, in south-central Yukon, well-preserved, Late Permian eclogite and glaucophane schist is exposed within quartzofeldspathic schist (Erdmer and Helmstaedt 1983; Erdmer 1987, 1992; Erdmer et al. 1998). Traditionally, the eclogite was assumed to have formed within the Slide Mountain terrane, a mid- to Late Paleozoic ocean basin that developed between the Yukon–Tanana arc and the western margin of North America (e.g. Tempelman-Kluit 1977, 1979; Monger et al. 1982; Wheeler et al. 1991; Colpron et al. 2006a, 2007).

The St. Cyr area is the least known of four localities that preserve Permian eclogite in the Yukon–Tanana terrane (Figs. 1, 2, and 3; Erdmer 1992). Eclogite, garnet amphibolite, and low-grade mafic and ultramafic rocks in the St. Cyr klippe, previously mapped as part of a tectonic mélange, were considered to have formed within the Slide Mountain oceanic crust during subduction of the back-arc region (Tempelman-Kluit 1979; Erdmer 1992). However, Erdmer et al. (1998) recognized that the Permian eclogite occurrences, including the St. Cyr localities, are hosted by quartzofeldspathic schist that seems to share a common metamorphic history. Mafic and ultramafic rocks of the Slide Mountain terrane, in contrast, are of much lower metamorphic grade and lack the muscovite and quartz-rich host rocks typical of the eclogite-bearing units at St. Cyr, Faro, Ross River, and Last Peak (Fig. 1; e.g. Wheeler et al. 1991; Colpron et al. 2006a). Because the Permian eclogite is preserved within structurally coherent units prior to peak metamorphism (Erdmer et al. 1998), it is not part of a chaotic distribution typical of a mélange. This discovery has led to our hypothesis that the Permian eclogite-bearing rocks are a crustal component of the Yukon–Tanana composite arc.

This study documents the extent of high-pressure metamorphism in the St. Cyr area and establishes the protoliths of eclogite and quartzofeldspathic schist in order to place these rocks into a regional tectonic context. Field relationships, petrology and mineral chemistry show that the occurrence of eclogite in the St. Cyr area is widespread and that the eclogite is part of a coherent unit of quartzofeldspathic schist that correlates with the Yukon–Tanana terrane, rather than the Slide Mountain terrane. U–Pb geochronology of metatonalite samples tie the protolith to the Klinkit phase of Yukon–Tanana arc building, and yields Permian metamorphic ages for the eclogite-facies event.

REGIONAL GEOLOGIC SETTING

The Yukon–Tanana terrane extends from Alaska to British Columbia, and constitutes a major component of the Peri-Laurentian allochthons within the northern Canadian Cordillera (Fig. 1; Colpron et al. 2006a, 2007). The terrane comprises a mid- to Late Paleozoic composite arc–forearc system built upon a sliver(s) of continental crust rifted from western Laurentia (Nelson et al. 2013 and references therein). Three Late Devonian to Late Permian, unconformity-bounded, geochronologically and geochemically distinct volcanic and volcaniclastic assemblages are built upon pre-Early Devonian metasedimentary basement known as the Snowcap assemblage (Fig. 1; Mortensen 1992; Piercey et al. 2002, 2006, 2012; Colpron et al. 2006a; Piercey and Colpron 2009). The Snowcap assemblage is a heterogeneous mix of psammitic, pelitic and calc-silicate schist, quartzite, marble and amphibolite (Colpron et al. 2006a, 2006b; Piercey and Colpron 2009). These rocks are typically polydeformed and polymetamorphosed up to amphibolite-facies conditions (Colpron et al. 2006a; Berman et al. 2007; Piercey and Colpron 2009; Staples et al. 2013). Mafic amphibolite in the Snowcap assemblage displays normal mid-ocean ridge basalt (N-MORB), enriched mid-ocean ridge basalt (E-MORB), or ocean island basalt (OIB) signatures consistent with emplacement in a continental rift setting (Nelson and Friedman 2004; Colpron et al. 2006b; Piercey and Colpron 2009). The Snowcap metasedimentary section is characterized

by Precambrian detrital zircon populations consistent with a western North American provenance (Piercey and Colpron 2009). Snowcap rocks are commonly intruded by deformed Late Devonian to Early Mississippian tonalite, granodiorite and granite bodies.

The Late Devonian to Early Mississippian Finlayson assemblage, the oldest arc assemblage, is characterized by mafic to felsic metavolcanic and metaplutonic rocks of arc and back-arc affinities (Murphy et al. 2006; Piercey et al. 2006, 2012). The assemblage also includes ultramafic rocks, carbonaceous pelite, quartzite, volcaniclastic rocks and minor marble (Mortensen 1992; Colpron et al. 2006a; Murphy et al. 2006). The Finlayson assemblage is unconformably overlain by the Mississippian to Early Permian Klinkit assemblage, consisting of variably metamorphosed mafic to intermediate calc-alkaline volcanic and volcaniclastic rocks with minor alkali basalt, limestone/marble and conglomerate (Simard et al. 2003; Nelson and Friedman 2004; Murphy et al. 2006; Roots et al. 2006). The Klondike assemblage, the youngest assemblage in the Yukon–Tanana terrane, consists of Middle to Late Permian felsic calc-alkaline metavolcanic and metaplutonic rocks and minor mafic rocks (Mortensen 1990; Dusel-Bacon et al. 2006).

Yukon–Tanana arc rocks are thought to have co-evolved with the opening of a marginal basin represented by an oceanic assemblage of chert, argillite and mafic volcanic rocks (Fig. 1; Mortensen 1992; Nelson 1993; Nelson et al. 2006; Colpron et al. 2006a; Piercey et al., 2006, 2012). This marginal basin was originally termed the Anvil Ocean by Tempelman-Kluit (1979).

The remnants of this basin are preserved today in a discontinuous belt along the eastern edge of the Yukon–Tanana terrane and called the Slide Mountain terrane (Wheeler and McFeely 1991; Mortensen 1992; Pigage 2004; Colpron et al. 2006a; Piercey et al. 2012). In southeastern Yukon, the Slide Mountain terrane is found as fault-bounded slivers of oceanic lithosphere preserved between the Yukon–Tanana terrane and the underlying North American margin. Representative assemblages of the Slide Mountain terrane include unmetamorphosed to greenschist-facies basalt, gabbro, leucogabbro, and variably serpentinized ultramafite, as well as deep-water sedimentary sequences such as chert and argillite (Tempelman-Kluit 1979; Colpron 2006; Colpron et al. 2006a; Murphy et al. 2006; Nelson et al. 2006; Piercey et al. 2012). Other sedimentary rocks found within the Slide Mountain terrane include siltstone, limestone, epiclastic sandstone and conglomerate, and phyllitic chert. Basalt typically display MORB geochemical signatures (Piercey et al. 2006), and together with the ultramafic rocks, is interpreted as a unit of oceanic crust and mantle (Murphy et al. 2006; Piercey et al 2012). Two important characteristics of the Slide Mountain terrane are that metamorphic grade is usually greenschist facies or lower and it is not known to contain muscovite–quartz schist (Wheeler et al. 1991; Colpron et al. 2006a; Piercey et al. 2012).

Blueschist- and eclogite-facies rocks are known from several localities in the Yukon–Tanana terrane (Fig. 1; Erdmer 1992; Mortensen 1992; Erdmer et al. 1998; Devine et al. 2006). The Simpson Range and Stewart Lake areas contain retrogressed eclogite that records evidence of mid-Mississippian high-pressure metamorphism (Creaser et al. 1999). In the
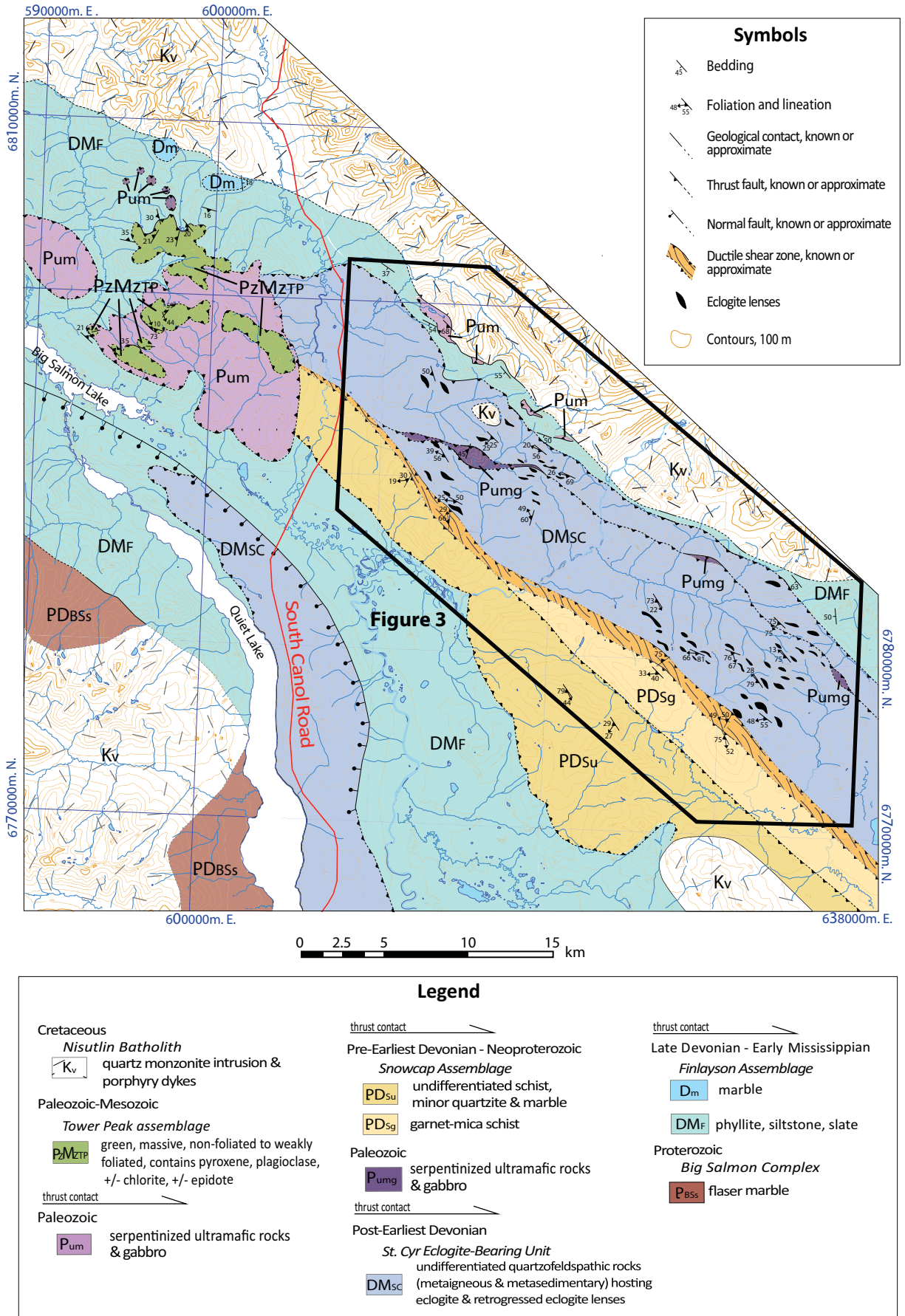
Figure 2. Geologic map of the Quiet Lake region, modified from Colpron (2006) and Tempelman-Kluit (2012), based on mapping by Isard (2014) and this study.
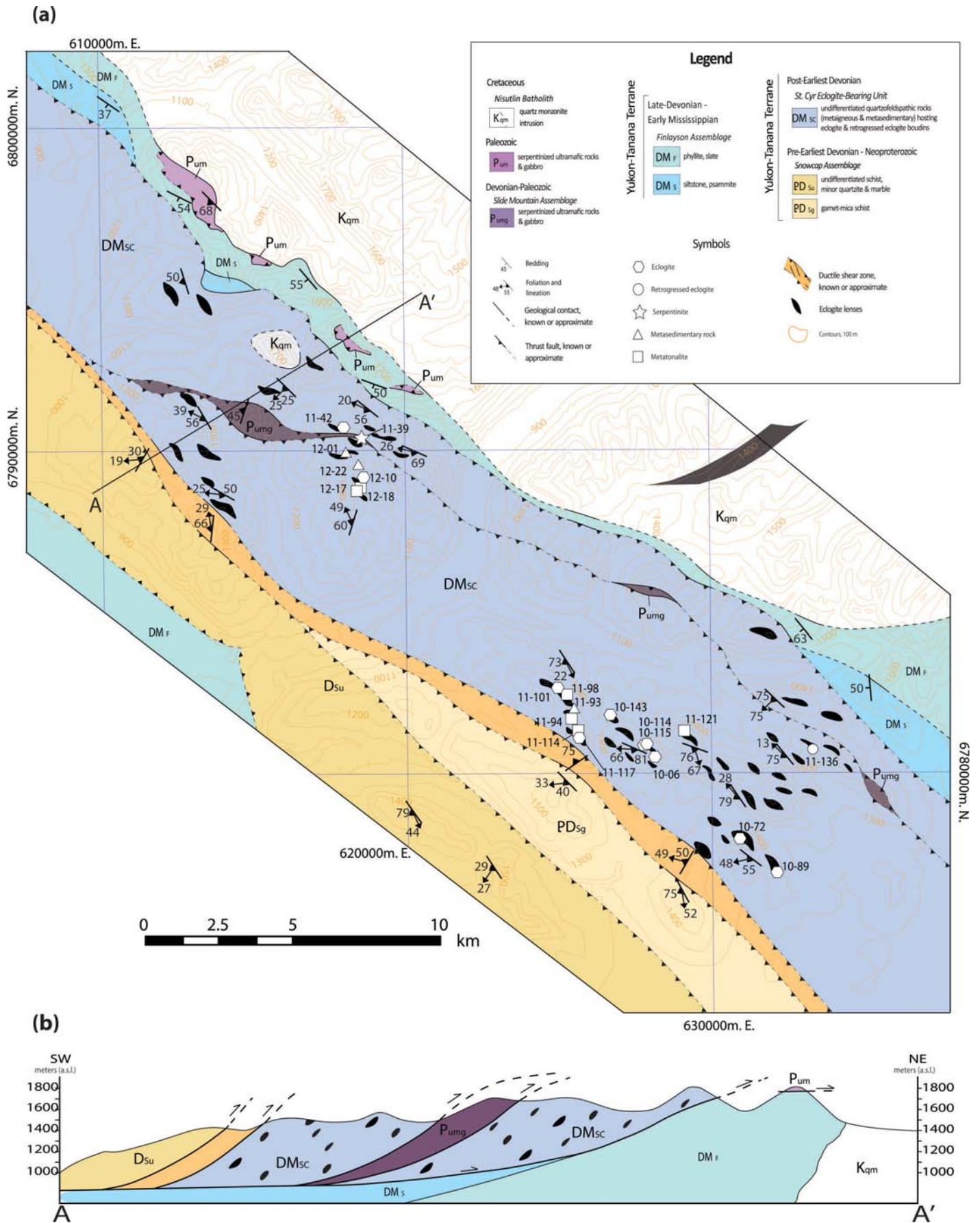
Figure 3. (a) Geologic map and (b) cross-section (vertical = horizontal scale) of the St. Cyr study area. UTM coordinates for samples shown on the map are found in Table DR-1.

southern Campbell Range, omphacite inclusions in zircon from garnet amphibolite are the only petrological evidence of high-pressure metamorphism within the Klatsa complex (Devine et al. 2006). These high-pressure mafic bodies are interpreted to have formed in a tectonic mélange with serpentinized ultramafic and gabbroic rocks and low-grade basalt, chert, limestone and chlorite-schist interpreted to be derived from Yukon–Tanana terrane basement and early Yukon–Tanana arc rocks (Erdmer 1987; Erdmer et al. 1998; Devine et al. 2006). In addition to the St. Cyr area, Permian age high-pressure rocks are found at Ross River, Faro and Last Peak (Erdmer and Armstrong 1989; Creaser et al. 1997; Erdmer et al. 1998). At these localities, eclogite and variably retrogressed equivalent rocks form metre- to tens of metres-sized lenses or structurally conformable layers hosted by greenschist-, blueschist-, or amphibolite-facies schist and quartzite (Erdmer and Helmstaedt 1983; Erdmer 1987; Erdmer et al. 1998). Structural fabrics shared by the eclogite and the host rocks led to the suggestion that they were in contact prior to peak metamorphism (Erdmer and Helmstaedt 1983; Erdmer 1987; Creaser et al. 1997; Erdmer et al. 1998).

GEOLOGY OF THE ST. CYR AREA
The eclogite-bearing rocks of the St. Cyr area are located southeast of the South Canol Road and 14 km northeast of Quiet Lake (Figs. 2 and 3). The area is bounded to the northeast by the Nisutlin Batholith. Eclogite, garnet amphibolite and moderately metamorphosed mafic and ultramafic rocks were previously interpreted as large blocks within a tectonic mélange assigned to the Slide Mountain terrane (Tempelman-Kluit 1979; Erdmer 1992). Fallas (1997) showed that eclogite and retrogressed eclogite are intercalated with quartzofeldspathic tectonites of both sedimentary and igneous origin, and that high-pressure metamorphism was much more widespread than previously known. Fallas (1997) also recognized the shared penetrative fabric displayed by quartzofeldspathic schist and eclogite.

Eclogite-Bearing Quartzofeldspathic Schist
Quartzofeldspathic schist hosting eclogite in the St. Cyr area occurs in at least two thrust slices in a 30 km long by 6 km wide, northwest-striking belt of metasedimentary and felsic metaigneous rocks that are intercalated on the metre to hundreds of metres scale. The quartzofeldspathic rocks were mapped as one unit because it was not always possible to distinguish between the two protoliths due to the strong foliation, fine grain size and poor exposure. Eclogite and retrogressed eclogite are found as sub-metre to hundreds of metres scale lenses surrounded by the quartzofeldspathic schist (Figs. 3 and 4). Both eclogite and the host rocks display schistosity in eclogite-facies assemblages. Schistosity in eclogite is defined by compositional layering and grain-shape-preferred orientation of omphacite and amphibole, whereas phengitic white mica defines the planar fabric of the schist. Lenses of eclogite are flattened parallel to the schistosity in the host rocks. Most commonly, schistosity in the mafic boudins is subparallel to the schistosity in the adjacent host rocks. In other cases, schistosity is discordant to the planar fabric in host rocks; some mafic boudins are massive or display complex internal folding.

Contacts between eclogite lenses and the surrounding host rocks range from sharp to gradational. Adjacent to contacts with the metasedimentary rocks, the mafic boudins preserve plagioclase melt stringers, which may be derived from prograde dehydration melting of the metasedimentary rocks or decompression melting of the metasedimentary rocks related to the boudinage of the high-pressure mafic rocks.

Quartzofeldspathic schist with an igneous origin include meta-quartz diorite, metatonalite and metatrondhjemite. Host rocks derived from sedimentary protoliths include mica- and garnet-bearing quartzite, garnet–mica schist and feldspar–quartz–mica schist. The schist is fine-grained and exhibits amphibolite- or greenschist-facies assemblages. Contacts between the metaigneous rocks and the metasedimentary rocks do not show evidence of faulting or strain localization and are assumed to be pre-metamorphic.

Schistosity of the quartzofeldspathic rocks is defined by the alignment of mica (including phengite) and, less commonly, grain-shape-preferred orientation of quartz. Intensity of fabric development is moderate to strong with few areas of localized strain. Schistosity in the upper and lower eclogite-bearing thrust sheets is dominantly northwest-striking and moderately to steeply southwest-dipping (Fig. 5). Poles to foliation in the upper sheet lie on a great circle and are interpreted to represent a later phase of regional-scale folding with an axis that plunges moderately to the northwest (Fig. 5a). Several macroscopic, open to isoclinal folds with moderately to steeply plunging, northwest-trending fold axes were observed, parasitic to the larger-scale fold; however, the data are inconclusive as to whether they form part of a regional synform, like that mapped by Tempelman-Kluit (1979, 2012), thus we did not include a synform in our cross-section. Quartz and plagioclase stretching lineations plunge moderately to steeply in the down-dip direction of the foliation plane, parallel to the fold axes (Fig. 5a). Lineations in the lower thrust sheet plunge shallowly to moderately toward the northwest or southeast (Fig. 5b).

Non-Eclogite-bearing Metasedimentary Units
In the southwestern part of the St. Cyr area, rocks with lithologic, metamorphic and detrital zircon signatures correlative with the Snowcap assemblage (Gilotti et al. 2013) are found in the hanging wall of a shear zone, structurally above eclogite-bearing quartzofeldspathic schist (PDsu and PDsg in Fig. 3). The rocks are divided into two lithostratigraphic units inferred to be separated by a northwest-striking thrust fault (Fig. 3). From west to east they include: (1) interlayered garnet–white mica schist, chlorite schist, quartz–white mica schist, with minor biotite schist, quartzite, calc-silicate and carbonate, and (2) garnet–white mica schist. The rocks are medium- to coarse-grained, variably deformed and exhibit amphibolite-facies metamorphism locally retrograded to greenschist-facies assemblages. The schistosity, defined by the planar alignment of micas, strikes northwest and dips moderately to steeply southwest (Fig. 5c). Quartz, mica and plagioclase stretching lineations are variable, plunging shallowly to the south and moderately to the northwest and southeast (Fig. 5c). Some garnet within the schist shows S-shaped spiral inclusion trails.
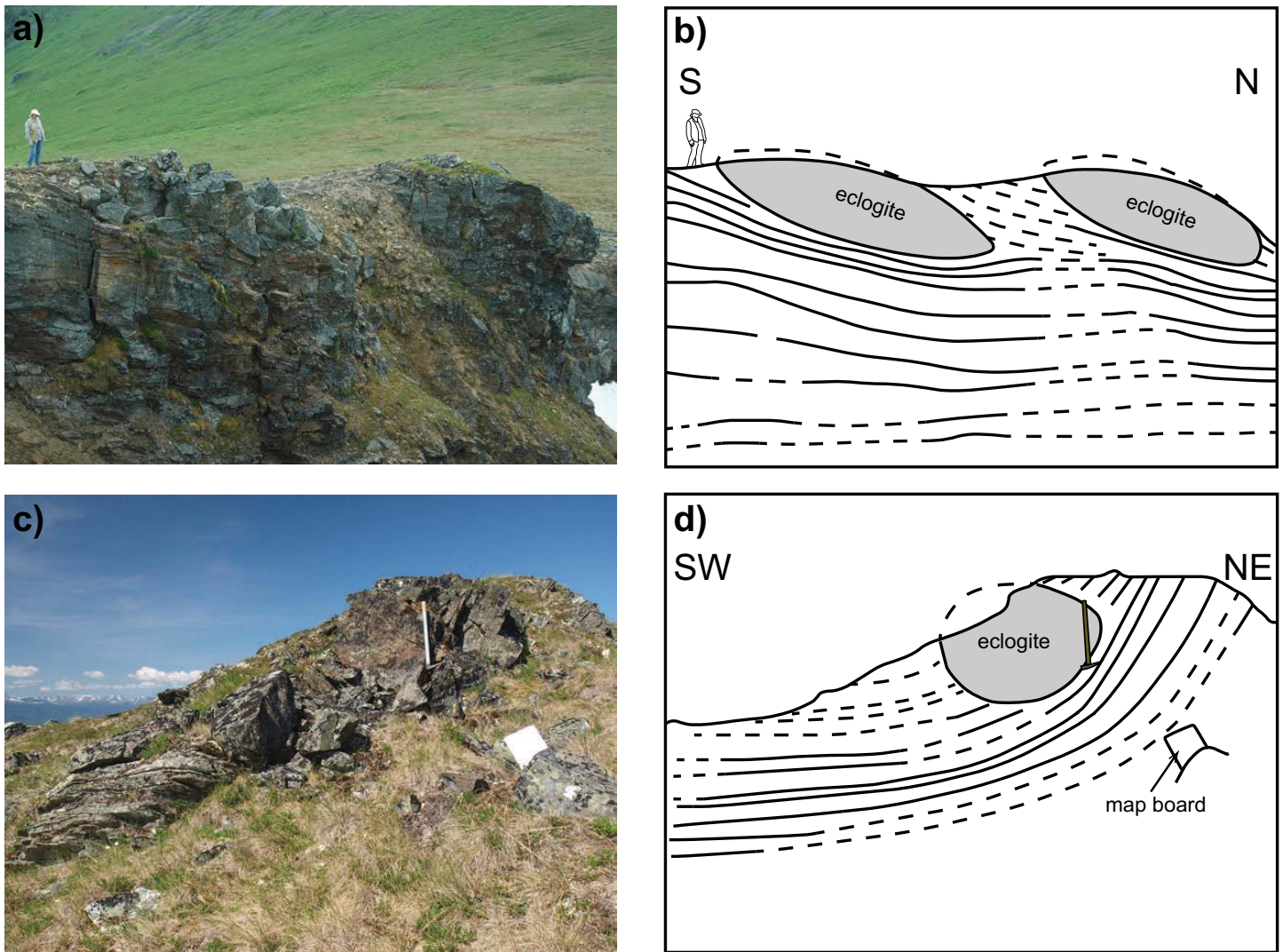
Figure 4. (a) and (c) Field photographs of eclogite boudins within the quartzofeldspathic host rocks. (a) Person for scale. (c) Hammer for scale is 80 cm long. (b) and (d) Line drawings showing the eclogite boudins and the trace of the foliation in the host rocks.

Shear Zone Between Eclogite-bearing Schist and Eclogite-free Schist

Eclogite-free metasedimentary rocks of Snowcap affinity lie structurally above a 400 m-thick shear zone separating this unit from underlying eclogite-bearing quartzofeldspathic schist (Figs. 2 and 3). The northwest-striking shear zone contains a mixture of metre-sized lenses of variably metamorphosed mafic, ultramafic, carbonate and undifferentiated quartzofeldspathic rocks in a matrix dominated by metapsammite. At least one lens of eclogite of indeterminate size was identified within the shear zone. The ultramafic rocks are pervasively serpentinized and mafic blocks are composed of greenschist-facies metagabbro. Quartzofeldspathic blocks contain garnet-bearing and garnet-free schist interpreted to be derived from sedimentary and felsic igneous protoliths, respectively. The metapsammitic matrix is composed of greenschist-facies phyllite and quartzite (Fig. 6). Outcrop-scale shear bands show a top-to-the-northeast thrust sense (Fig. 6a and b).

Foliation in the metapsammitic matrix is defined by the planar alignment of phyllosilicate minerals. Foliation strikes northwest or northeast and dips moderately to steeply to the southwest, northwest and northeast (Fig. 5d). Quartz, mica and plagioclase stretching lineations plunge down-dip or moderately to steeply northwest (Fig. 5d). These rocks are complexly folded on the centimetre to metre scale, with randomly oriented, but steeply plunging fold axes (Fig. 6c and d).

Low-Grade Mafic and Ultramafic Rocks

Mafic and ultramafic rocks form a structurally imbricated panel within the eclogite-bearing quartzofeldspathic unit (Pumg; Fig. 3). The ultramafic rocks form prominent orange peaks on high ridges throughout the field area (Fig. 7a). These fault-bounded bodies range in size from a few square metres to several hundred square metres and include both greenschist-facies gabbro to leucogabbro and intact, variably serpentinized ultramafic rocks composed of olivine + clinopyroxene. Powder X-ray diffraction analysis of serpentinite sample 11-39 on a D8 Advance Bruker instrument housed within the Department of Chemistry, University of Iowa, shows that lizardite is the main serpentine mineral, and as such indicates metamorphic temperatures < 300°C (Evans et al. 2013). Lizardite was also identified in the northwestern portion of the St. Cyr klippe, northwest of South Canol Road (Isard and Gilotti 2014). Within the centres of the panels, metamor-
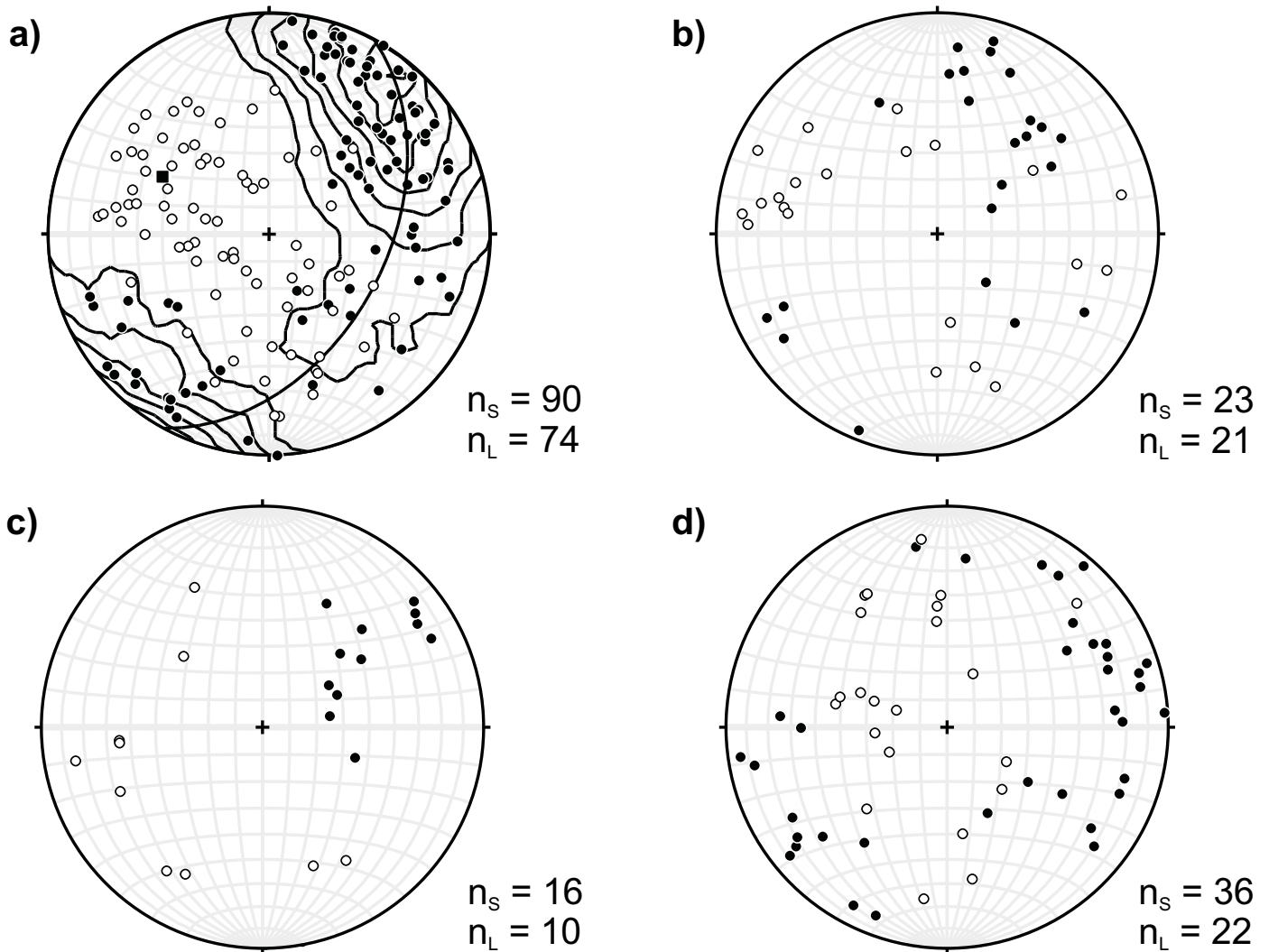
Figure 5. Lower hemisphere, equal area stereonet of poles to foliation (filled circles) and lineations (open circles) in the field area. (a) Upper thrust sheet of eclogite-bearing quartzofeldspathic schist. Poles to foliations plot along a great circle whose pole (black square) gives the regional fold axis at 298°/45°. (b) Lower thrust sheet of eclogite-bearing quartzofeldspathic schist. (c) Non-eclogite-bearing schist assigned to the Snowcap assemblage. (d) Shear zone between eclogite-bearing and non-eclogite-bearing schist.

phosed gabbro and leucogabbro is massive and exhibits igneous textures (Fig. 7b), with leucogabbro intruded into the surrounding gabbro and ultramafic rocks (Fig. 7c). Adjacent to the fault contacts, ultramafic rocks are moderately to strongly foliated, dipping steeply to the southwest; the degree of deformation increases with the degree of serpentinization and proximity to the faults. Although the mafic and ultramafic protoliths are inferred to be largely Paleozoic in age, this interpretation is complicated by the recovery of unexpected Mesozoic zircon from several units on both sides of the South Canol Road (Isard 2014; W.C. McClelland unpublished data).

Finlayson Assemblage and Nisutlin Batholith

The footwall of the St. Cyr klippe (Fig. 3) contains siliciclastic and minor carbonate rocks of the Finlayson assemblage, the oldest volcanic and volcaniclastic arc assemblage of the Yukon–Tanana terrane (Colpron et al. 2006a). The contact with the overlying eclogite-bearing schist is sharp, and both schist and clastic sedimentary rocks are brecciated. The siliciclastic rocks in the footwall consist of an interlayered package of phyllite, siltstone, shale, with minor psammite overlain by

thickly-bedded psammite, quartzite, marble and minor siltstone. A detrital zircon population from marble in the footwall yielded a maximum depositional age of 368 Ma, supporting the interpretation that the footwall is part of the Finlayson assemblage of the Yukon–Tanana terrane (Isard 2014). The low-grade metasedimentary rocks in the footwall contain a pervasive, moderately southwest-dipping cleavage.

The Early to mid-Cretaceous Nisutlin Batholith cuts rocks of both the Finlayson assemblage and St. Cyr klippe (Tempelman-Kluit 1977; Colpron 2006). Intrusion of medium- to coarse-grained, biotite quartz monzonite produced a 100 m-thick contact aureole that metamorphosed the Finlayson sedimentary rocks to andalusite-bearing hornfels (Fallas et al. 1999). A small 1x1 km satellite pluton of the Nisutlin Batholith intruded quartzofeldspathic schist in the central-eastern portion of the field area, pinning movement on the basal thrust of the St. Cyr klippe as pre-Cretaceous in age.

Structural Interpretation

The Snowcap assemblage, the St. Cyr eclogite-bearing unit and the mafic–ultramafic rocks form a series of thrust slices, inter-
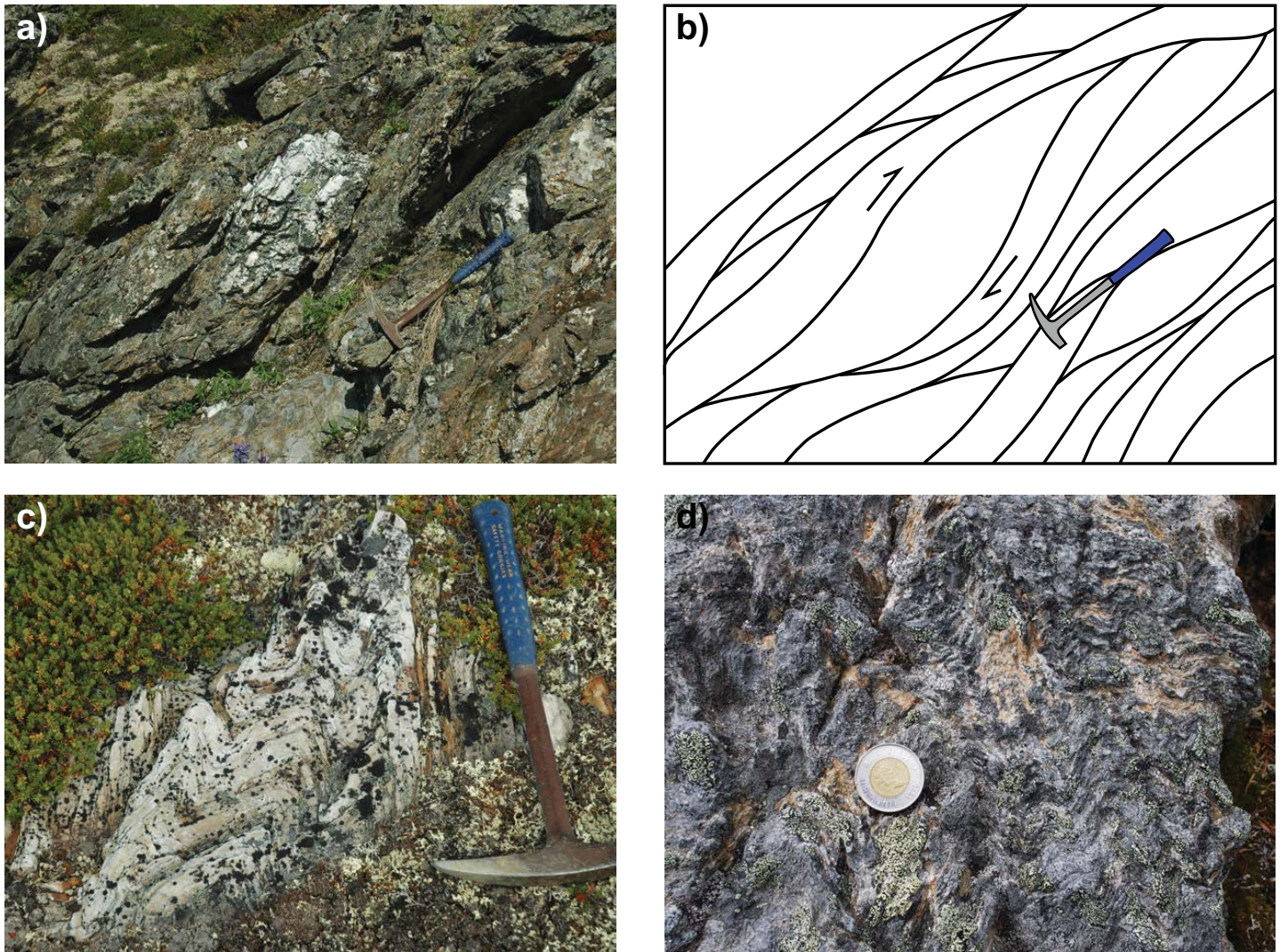
Figure 6. Field photographs of the metapsammitic matrix of the shear zone. (a) View of the southwest-dipping foliation from the northwestern portion of the field area. Hammer for scale is 42 cm long. (b) Line drawing of photo in (a) illustrating an anastomosing foliation and top-to-the-northeast direction of movement. (c) Folded quartzite; hammer is 42 cm long. (d) Crenulations within a micaceous quartzite. Coin for scale is 2.8 cm in diameter.

preted as an imbricate stack (see cross-section A–A' in Fig. 3). The ductile shear zone with top-to-the-northeast sense of shear clearly places slices of Snowcap assemblage over eclogite-bearing schist. However, the eclogite-bearing unit forms two distinct, southwest-dipping slices that are separated by a younger thrust carrying the mafic and ultramafic rocks, which potentially contain Mesozoic gabbro. The imbricate stack is overlain by a composite klippe of mafic, ultramafic and serpentinite lithologies and the uppermost Tower Peak unit – a low-grade metabasalt (Fig. 2; Isard 2014). Both the Tower Peak and mafic–ultramafic units exhibit brittle structures, including fault gouge and cataclasite, and are metamorphosed in the greenschist facies. Mesozoic zircon has also been recovered from the Tower Peak metabasalt (Isard 2014). We have chosen to map the two mafic–ultramafic units separately (Figs. 2 and 3; Pum and Pumg) based on their structural level, but we acknowledge that they could share the same protolith.

The imbricate slices and the uppermost klippe appear to have a common footwall dominated by phyllite (Fig. 2). Templeman-Kluit (1979, 2012) mapped the entire structure as the St. Cyr klippe, but this interpretation hinges on the nature of

the southwestern contact between the upper slice of the Snowcap assemblage (PDSu; Fig. 2) and the phyllite. We did not observe an exposure of this key contact; therefore, we kept the relationship shown in the previous map that requires a sub-horizontal thrust beneath the imbricate slices. We cannot confirm that the entire structure is a klippe, but the alternative interpretation of Finlayson assemblage thrust over Snowcap assemblage would require a thrust within the current footwall (DMF) northwest of Tower Peak, which was also not observed (Fig. 2).

PETROLOGY OF ECLOGITE AND QUARTZOFELDSPATHIC HOST ROCKS

Eclogitic rocks from two localities near the South Canol Road were first described by Erdmer (1992); additional localities were noted by Fallas et al. (1998). Here, we document the pervasive nature of high-pressure metamorphism of both the mafic lenses and the quartzofeldspathic host rocks in the St. Cyr area. Omphacite, garnet, quartz and rutile comprise the representative high-pressure assemblage for mafic rocks, whereas the presence of phengite and garnet is the most com-
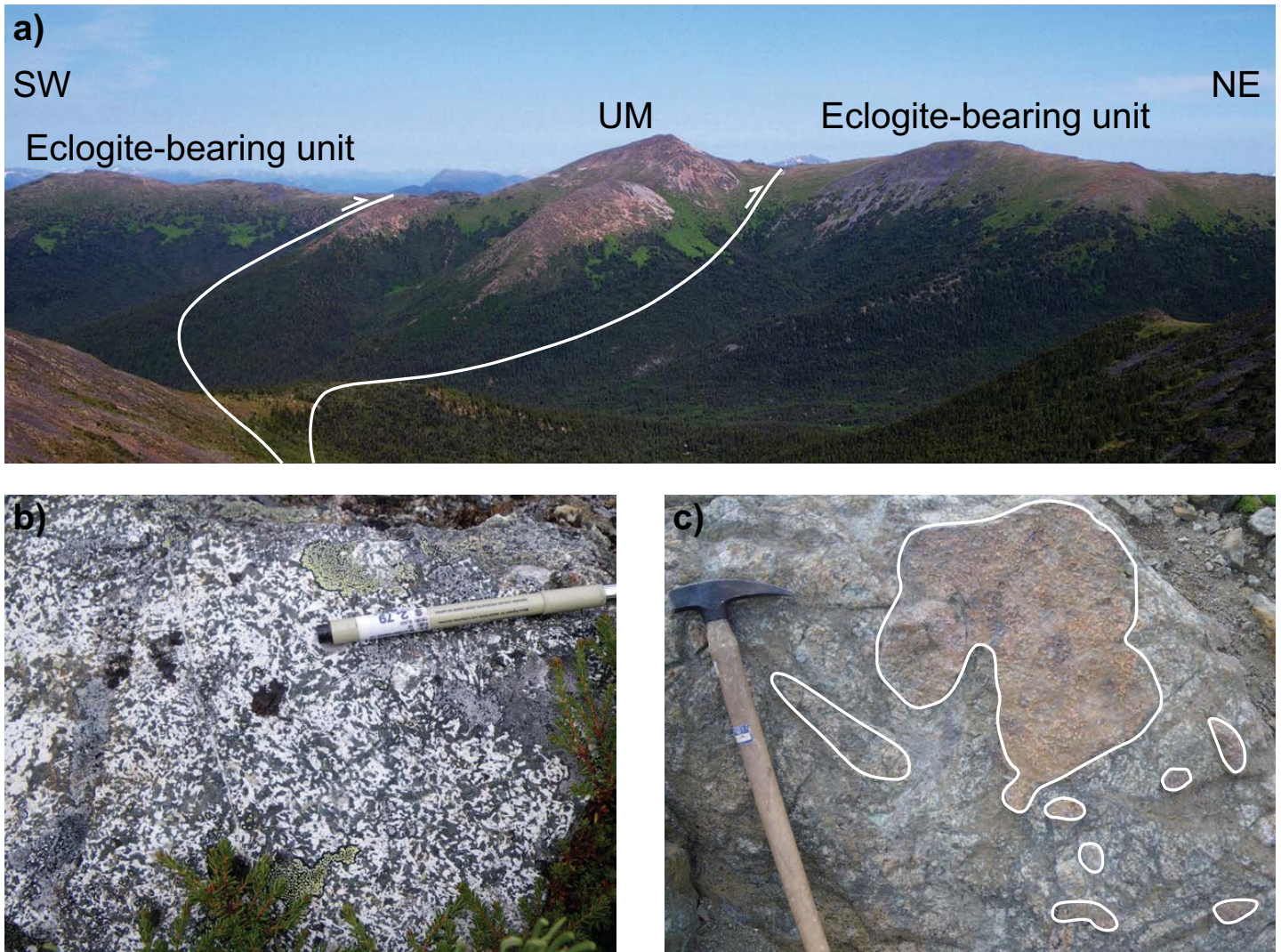
Figure 7. Field photographs of low-grade mafic and ultramafic rocks imbricated within the St. Cyr eclogite-bearing unit. (a) View of a large, orange-weathering ultramafic body (UM) in the central portion of the field area. This photo looks northwest at the cross-section line in Figure 3b. White lines mark thrust boundaries. (b) Outcrop of leuco-gabbro preserving intrusive igneous texture. Pen for scale is 13.5 cm long. (c) Outcrop of leucogabbro intrusion with ultramafic enclaves (outlined in white). Hammer for scale is 80 cm long.

pelling evidence of high-pressure metamorphism in quartzofeldspathic schist. Both assemblages display an amphibolite-facies to greenschist-facies overprint.

Eclogite and Retrogressed Eclogite

Well-preserved eclogite contains a peak mineral assemblage of omphacite + garnet + quartz + rutile ± phengite ± amphibole, with epidote, apatite and zircon as accessory phases (Fig. 8). Omphacite forms pale green, 200–800 μm equant grains or elongate porphyroblasts. Garnet is typically idioblastic and fine-grained, ≤ 300 mm in diameter. Where present as a peak phase, brownish-green amphibole constitutes subidioblastic, 300–900 μm grains in equilibrium with omphacite or idioblastic inclusions in garnet (Fig. 8b). Rutile is present in the matrix and included within garnet. Other inclusions observed in garnet are omphacite, quartz, titanite, plagioclase, diopside, augite, phengite, muscovite, epidote, ilmenite and calcite; these inclusions are generally confined to the garnet cores. Quartz occurs as either 100–300 μm long grains with undulose-extinction and subgrains, or < 100 μm polycrystalline aggregates with undu-

lose- to flat-extinction and 120° triple-junctions.

Eclogite shows progressive retrogression from fresh eclogite to garnet amphibolite. In the transition zones between preserved eclogite and garnet amphibolite, omphacite-rich and amphibole-rich layers are commonly interleaved. In the least retrogressed samples, omphacite is replaced by fine-grained, lobate symplectites of diopside + plagioclase or amphibole + plagioclase (Fig. 8c and d). Phengite is commonly replaced by fine-grained, blocky symplectites of biotite and plagioclase. Other retrograde features include rutile rimmed by ilmenite, ilmenite surrounded by titanite and garnet rimmed by biotite. In moderately retrogressed samples, garnet is subhedral, with embayed edges converted to biotite, and inclusions of quartz, amphibole, rutile, clinopyroxene and phengite. In samples with ≥ 10 modal percent clinopyroxene, amphibole forms medium, light greenish-brown, subidioblastic to idioblastic grains, with long dimensions that help define the schistosity. In samples with trace amounts of clinopyroxene, the clinopyroxene is typically small (< 50 μm) and surrounded by extremely fine-grained amphibole + plagioclase symplectite. The symplectite
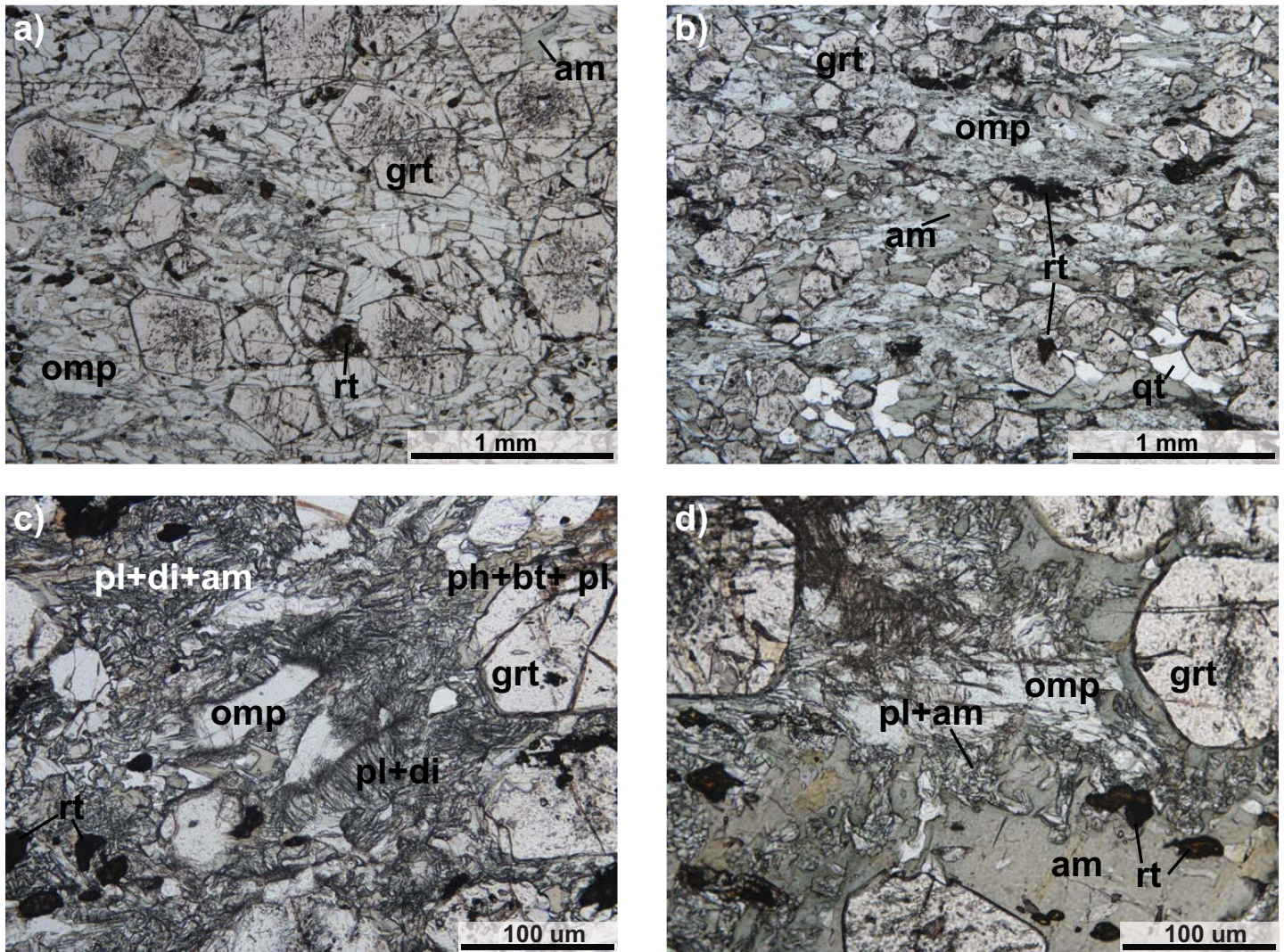
Figure 8. Photomicrographs of eclogite in the St. Cyr klippe. (a) Well-preserved eclogite sample 11-101 with a peak assemblage of omphacite, garnet and rutile. (b) Well-preserved eclogite sample 10-89 with a peak assemblage of omphacite, garnet, quartz, amphibole and rutile. (c) Retrogressed eclogite sample 12-10 showing omphacite altering to lobate symplectite of plagioclase + diopside, which is in turn replaced by amphibole. (d) Retrogressed eclogite sample 10-06 with omphacite partially converted to plagioclase + amphibole. Plane polarized light. am = amphibole, bt = biotite, di = diopside, grt = garnet, omp = omphacite, pl = plagioclase, qt = quartz, rt = rutile.

creates a cloudy appearance along the grain boundaries of larger amphibole grains. Completely retrogressed eclogite consists of amphibole + garnet + plagioclase ± quartz ± biotite ± ilmenite ± titanite. Retrograde amphibole is pale bluish-green, 200–800 μm, with a grain-shape-preferred orientation parallel to the foliation, and straight grain boundaries devoid of any symplectite. Quartz and amphibole are common inclusions in garnet.

Quartzofeldspathic Schist
Quartzofeldspathic schist is derived from both igneous and sedimentary protoliths. The mineral assemblage of metaigneous schist is quartz, garnet, phengite and plagioclase, with or without biotite, clinozoisite, or apatite (Fig. 9a and b). Rutile, apatite, ilmenite and K-feldspar are common accessory phases. Metasedimentary protoliths are distinguished from metaigneous rocks by a higher modal percent of quartz, garnet, micas and a lack of K-feldspar. In both lithologies, quartz exhibits undulose-extinction, subgrains and lobate grain boundaries – evidence for dynamic recrystallization over a range of temper-

atures (~300–500°C; e.g. Stipp et al. 2002). Coarse-grained biotite is pale reddish-brown to dark greenish-brown and is commonly altered to chlorite. Biotite is also a typical retrograde phase after phengite.

In metaigneous rocks (Fig. 9a and b), phengite grains are either 300–800 μm in length, isolated grains within the matrix, or occur as < 50 μm, idioblastic, randomly-oriented crystals replacing plagioclase. Garnet is present as subidioblastic porphyroblasts with embayed boundaries altered to chlorite. Titanite forms inclusions in garnet or overgrowths on ilmenite or rutile. Clinozoisite is 100–400 μm long and exhibits embayed grain boundaries. Epidote forms < 50 μm lobes replacing clinozoisite and plagioclase, which consists of 500–1000 μm grains with embayed boundaries and multiple phases of albite growth and deformation twins.

In metasedimentary rocks (Fig. 9c and d), 100–600 μm phengite is a common matrix phase. Garnet forms isolated, subidioblastic to rounded porphyroblasts or aggregates of small, ≤ 100 μm, grains within plagioclase and contains inclusions of quartz, phengite and biotite. In the most retrogressed
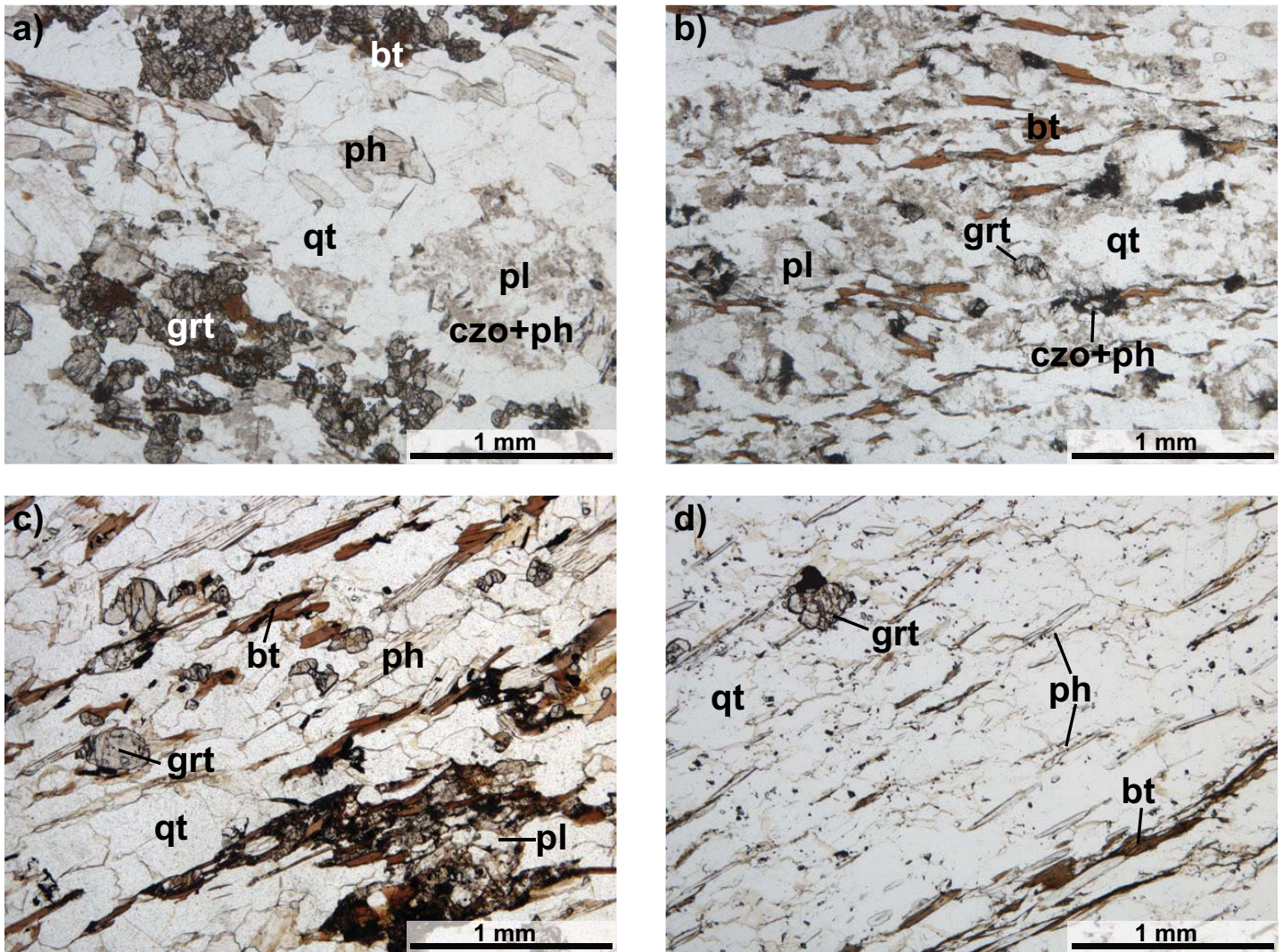
Figure 9. Photomicrographs of the quartzofeldspathic host rocks. (a) Garnet-bearing, phengite + biotite-bearing metatonalite sample 11-121. Plagioclase is replaced by fine-grained phengite and clinozoisite. (b) Foliated metatonalite sample 11-98. This sample has more biotite than sample 11-121 and phengite occurs within or adjacent to plagioclase. (c) Sample 11-93, garnet–mica schist with phengite. (d) Garnet–phengite quartzite sample 12-01. Plane-polarized light. bt = biotite, czo = clinozoisite, grt = garnet, ph = phengite, pl = plagioclase, qt = quartz.

samples, garnet is fractured and replaced by chlorite or biotite. In quartzite, the long axes of garnet grains lie in the schistosity defined by the grain-shape-preferred orientation of micas. Titanite forms medium, idioblastic grains within the matrix. Plagioclase is found as elliptical porphyroclasts with embayed or lobate grain boundaries. Quartz in plagioclase-rich samples is also preserved as porphyroclasts, surrounded by a finer grained quartz + mica matrix.

MINERAL CHEMISTRY

Mineral composition was determined for nine eclogite, three metatonalite and three metasedimentary rocks in order to characterize the high-pressure phases. UTM coordinates for the analyzed samples are shown in Table DR-1[1], and representative mineral compositions are given in Tables 1, 2, DR-2, DR-3, and DR-4. Mineral chemistry was determined using a CAME-

CA SX-100 electron microprobe at the University of California, Davis. Analytical conditions include 15 kV acceleration voltage, 5–20 nA beam current and a beam diameter of 1–10 mm. Major element concentrations are shown as weight % oxides (wt.%). Amphibole nomenclature is after Hawthorne et al. (2012), pyroxene nomenclature is after Morimoto (1989) and epidote nomenclature follows Armbruster et al. (2006). Mineral abbreviations are from Whitney and Evans (2010).

Clinopyroxene

Clinopyroxene composition is plotted in Figure 10 and representative analyses are given in Table 1. Clinopyroxene analyses were normalized to four cations per formula unit ($M2M1Si_2O_6$) and the Fe^{2+}/Fe^{3+} ratio was obtained from the charge balance. Cations were assigned to the M1 and M2 sites according to the procedure described in Morimoto (1989).

[1]Electronic supplementary materials (Tables DR-1 through -8), are available at the GAC's open source GC Data Repository, Andrew Hynes Series link, at http://www.gac.ca/wp/?page_id=306.

Table 1. Representative clinopyroxene composition in eclogite.

Sample	10-115	12-10	11-42	12-10	11-117	11-42	11-117	11-42
Mineral	Omp in matrix	Omp in matrix	Omp in matrix	Cpx within symplectite	Cpx within symplectite	Cpx adj to am+pl symplectite	Omp incl in garnet	Cpx incl in garnet
Analysis #	3/1	2/1	12/1	6/1	5/1	9/1	4/1	3/1
SiO_2	55.866	54.393	53.995	51.107	53.655	53.150	55.152	52.887
TiO_2	0.060	0.203	0.082	0.322	0.075	0.187	0.178	0.147
Al_2O_3	10.262	9.723	4.726	7.697	1.679	3.960	9.981	1.487
Cr_2O_3		0.045		0.033	0.009			
FeO	5.520	5.189	7.108	6.441	11.260	7.441	6.436	9.679
MnO	0.000	0.048	0.175	0.048	0.177	0.173	0.078	0.408
MgO	8.049	9.334	11.433	12.757	10.673	12.043	8.142	12.205
CaO	13.457	16.073	19.398	18.837	21.570	20.841	13.560	23.113
Na_2O	6.780	5.207	2.865	2.296	1.416	2.290	6.398	0.409
K_2O	0.000		0.005			0.017	0.001	0.100
Wt % total	99.994	100.215	99.787	99.538	100.514	100.102	99.926	100.435
Mineral formulas based on 6 oxygens								
Si	1.992	1.949	1.980	1.867	2.005	1.949	1.977	1.976
Ti	0.002	0.005	0.002	0.009	0.002	0.005	0.005	0.004
Al	0.431	0.411	0.204	0.331	0.074	0.171	0.422	0.065
Cr		0.001		0.001	0.000			
Fe^{3+}	0.050	0.041	0.036	0.080	0.014	0.084	0.059	0.009
Fe^{2+}	0.114	0.114	0.182	0.117	0.338	0.145	0.134	0.293
Mn	0.000	0.001	0.005	0.001	0.006	0.005	0.002	0.013
Mg	0.428	0.499	0.625	0.695	0.595	0.658	0.435	0.680
Ca	0.514	0.617	0.762	0.737	0.864	0.819	0.521	0.925
Na	0.469	0.362	0.204	0.163	0.103	0.163	0.445	0.030
K	0.000		0.000			0.001	0.000	0.005
End Member for Ca-Na Pyroxenes (Morimoto 1989)								
Quad	0.50	0.60	0.76	0.75	0.88	0.77	0.51	0.96
Jd	0.45	0.35	0.20	0.17	0.10	0.15	0.43	0.03
Ae	0.05	0.04	0.04	0.08	0.01	0.08	0.06	0.01
Quad Cpx for Ws-En-Fs plot								
Wo				0.45	0.48	0.48		0.49
En				0.43	0.33	0.39		0.36
Fs				0.12	0.19	0.13		0.16

am – amphibole, cpx – clinopyroxene, omp – omphacite, pl - plagioclase.

Omphacite (i.e. sodic clinopyroxene with a jadeite component between 20–80 mol %) was confirmed in all nine eclogite samples. In general, $Jd_{35–49}$ in grain cores decreases to $Jd_{20–30}$ at grain rims, which are adjacent to symplectites. Diopside is found within symplectites or at grain rims adjacent to amphibole–plagioclase symplectites with a jadeite content ranging from $Jd_{10–18}$. Idioblastic clinopyroxene inclusions in garnet are diopside ($Jd_{2–8}$) or omphacite ($Jd_{20–43}$).

Amphibole
Taramite, kataphorite and winchite [Si = 6.16–7.21 atoms per formula unit (apfu), Ca = 1.13–1.49 apfu, [A](Na+K) = 0.34–0.86 apfu] are found as matrix grains in equilibrium with omphacite (Fig. 11; Table DR-2). Symplectitic amphibole is more calcic than the matrix amphibole, and is pargasitic with Si = 6.30–7.19 apfu, Ca = 1.50–2.28 apfu, [A](Na+K) = 0.48–0.90 apfu. Both Na–Ca and Ca amphibole are included in garnet. These include taramite and katophorite [Si = 6.00–6.72 apfu, Ca = 1.50–1.31 apfu, [A](Na+K) = 0.53–0.88 apfu] as sodic phases, and sadanagite, pargasite and magnesiohornblende [Si = 5.87–6.89 apfu, Ca = 1.51–1.79 apfu, [A](Na+K) = 0.34–0.81 apfu] as calcic phases.

Garnet
Garnet in eclogite exhibits a rather narrow compositional range of almandine–pyrope–grossular–spessartine solid solution from $Alm_{50–61}Prp_{7–21}Grs_{17–34}Sps_{0.5–6.8}$ (Table DR-3). Garnet is typical of type C eclogite, which is defined by Coleman et al. (1965) as crustally derived, relatively low-temperature eclogite. Garnet displays both prograde and sector zoning (Fig. 12). Prograde compositional zoning exhibits a core to rim decrease in Mn and Ca. In some cases, Ca zonation is more complex, rising away from the core before decreasing at the rim. Sector zoning is developed in the intermediate domain between a distinct core and outer rim, and is thought to be due to either the heterogeneous distribution of Mg and Fe on the {110} faces

Table 2. Representative phengite composition.

| Rock type	Eclogite			Metatonalite		Metasedimentary rock		
Sample	11-117	10-115	10-115	11-94	12-18	11-93	11-93	12-22
Mineral	Ph in matrix core	Ph in matrix rim	Ph incl in Grt	Ph in matrix	Ph repl Pl	Ph in matrix	Ph incl in Grt	Ph repl Pl
Analysis #	1/13	3/1	1/1	1/5	1/1	7/1	1/1	7/1
SiO_2	49.642	48.466	49.049	47.900	50.863	48.283	46.879	48.283
TiO_2	0.879	0.974	0.995	0.811	0.054	1.310	1.518	0.000
Al_2O_3	27.241	27.593	28.004	30.459	27.479	29.088	32.298	28.680
FeO	2.356	2.274	2.488	1.683	2.188	3.416	1.746	2.035
MnO	0.011	0.011	0.000	0.000	0.000	0.034	0.000	0.069
MgO	3.319	3.374	3.556	2.278	2.325	2.730	2.064	2.940
CaO	0.011	0.030	0.014	0.029	0.128	0.000	0.003	0.077
Na_2O	0.630	0.524	0.688	0.307	2.104	0.496	0.717	0.739
K_2O	10.289	9.945	9.853	10.506	8.482	9.892	9.826	9.721
BaO		0.876			0.630	0.617	0.610	0.856	0.683
Wt % total	94.378	94.067	94.647	94.603	94.240	95.859	95.907	93.227
Mineral formulas based on 11 oxygens								
Si	3.353	3.304	3.301	3.234	3.422	3.240	3.127	3.306
Ti	0.045	0.050	0.050	0.041	0.003	0.066	0.076	0.000
Al	2.168	2.217	2.221	2.423	2.179	2.300	2.538	2.314
Fe^{2+}	0.133	0.130	0.140	0.095	0.123	0.192	0.097	0.116
Mn	0.001	0.001	0.000	0.000	0.000	0.002	0.000	0.004
Mg	0.334	0.343	0.357	0.229	0.233	0.273	0.205	0.300
Ca	0.001	0.002	0.001	0.002	0.009	0.000	0.000	0.006
Na	0.082	0.069	0.090	0.040	0.274	0.065	0.093	0.098
K	0.886	0.865	0.846	0.905	0.728	0.847	0.836	0.849
Ba		0.023		0.017	0.016	0.016	0.022	0.018

grt – garnet, ph – phengite, pl - plagioclase.
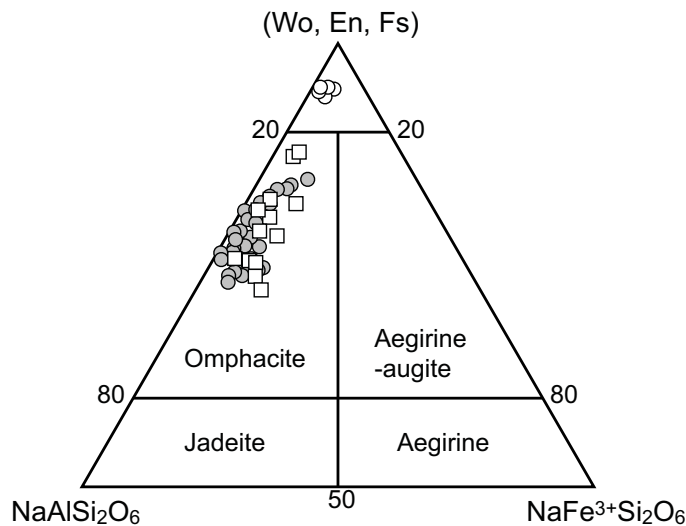
Figure 10. Ternary plots (after Morimoto 1989) of omphacite composition in the matrix (grey circles), included in garnet (open squares), and diopside in symplectite (open circles). Wo, En, Fs = wollastonite (Fe: $CaSiO_3$) + enstatite (En: $MgSiO_3$) + ferrosilite (Fs: $FeSiO_3$).

early in growth history, only to steeply increase at the rim. Mn shows less well-defined sector variation in some samples. The ~30 μm-wide rim of the grain is characterized by a slight increase in Mn, and decrease in Fe and Ca.

Garnet in quartzofeldspathic schist is much more compositionally complex than that in the eclogite (Table DR-3). Grains display highly variable zoning patterns in metasedimentary and metaigneous schist, and even between garnet grains in the same sample. This may reflect the original bulk rock composition or some of the garnet could be detrital. Zoning along rims and cracks indicates that garnet has been affected by element diffusion after peak metamorphism. In general, garnet in metatonalite is a solid solution in the range $Alm_{39-54}Prp_{1.2-25}Grs_{29-51}Sps_{2.7-7.1}$. Although pyrope content reaches 25 mol%, most contains less than 2 mol%. Metatonalite garnet displays two types of zoning: (1) homogeneous cores with <20 μm wide retrograde rims where Fe and Mn increase and Mg decreases, and (2) prograde zoning with a core to rim increase in Mg and decrease in Fe, Ca and Mn without a retrograde rim. Garnet composition in the metasedimentary rocks is $Alm_{54-69}Prp_{6-21}Grs_{10-29}Sps_{0.5-21}$. These garnet grains are irregularly zoned and tend to be more Mn-rich than garnet in metatonalite; they generally exhibit a core to rim decrease in Fe and Mg and increase in Mn and Ca. At the outermost rims (<20 μm from the edge) Fe and Mg show significant decreas-

of garnet or a rapid increase in temperature (Shirahata and Hirajima 1995; Kleinschmidt et al. 2008). Sector zoning is most pronounced in the Mg component, where Mg decreases

a)
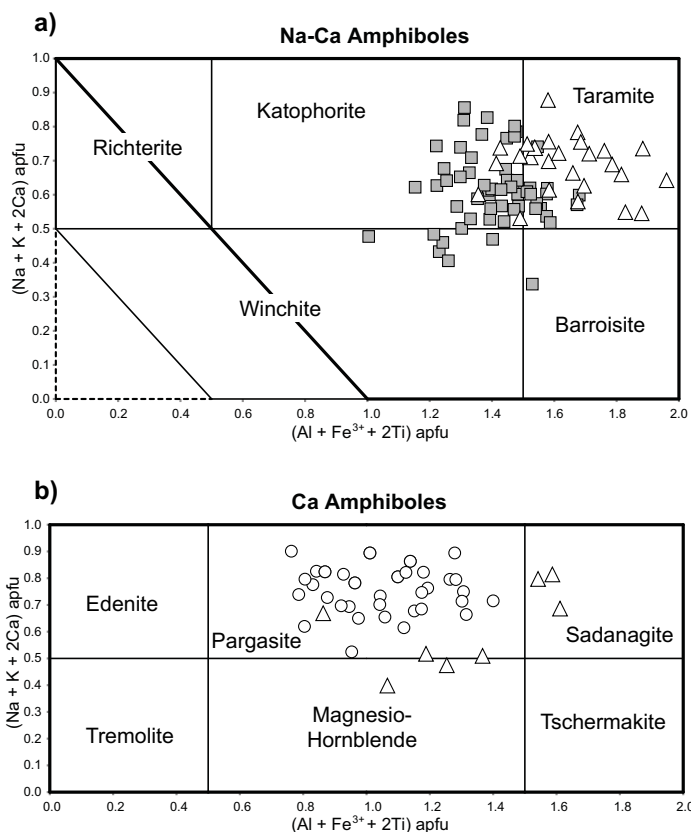

Na-Ca Amphiboles

b)

Ca Amphiboles

Figure 11. Amphibole composition; diagrams after Hawthorne et al. (2012). (a) Na–Ca amphibole in the matrix (grey squares) and included in garnet (open triangles). (b) Ca-amphibole in symplectites (open circles) and as garnet inclusions (open triangles).

a)   **b)**

Figure 12. Mg X-ray maps in sector-zoned garnet from the St. Cyr klippe. Eclogite samples (a) 10-143 and (b) 10-06. Warm colors represent higher elemental concentrations.

Figure 13. Backscattered electron SEM image of fine-grained phengite replacing plagioclase within metatonalite sample 12-18.

es in concentration. For example, Fe decreases as much as 39 mol% from the adjacent analysis in the core of the grain, whereas Ca and Mn substantially increase – 22 mol% in the case of Ca. Along cracks, Mg decreases, Ca and Mn increase and Fe remains unchanged.

Phengite

White mica is muscovite to phengite (Si apfu > 3.2) in chemical composition. Phengite was found in three eclogite samples as matrix grains and included in garnet. In the matrix, white mica composition ranges from 3.12 to 3.67 Si apfu (Table 2). Inclusions in garnet have Si contents as high as 3.32 apfu. Although most of the phengite is homogeneous, a few grains in each sample display a decrease in Mg, Ba and Si within 25–10 μm of the grain rim. Matrix phengite was identified in all six of the analyzed quartzofeldspathic host rocks, where it is irregularly zoned, with the highest values of Si generally concentrated in grain cores. With decreasing Si, Ba and Mg also decrease. In metatonalite, matrix white mica contains 3.07 to 3.45 Si apfu, and the fine grains of phengite that replace plagioclase contain up to 3.48 Si apfu (Fig. 13; Table 2). In metasedimentary rocks, Si concentrations are 3.04 to 3.34 apfu, which is lower than the Si content in metatonalite, possibly a reflection of different bulk composition. White mica inclusions in garnet in metasedimentary rocks are muscovite, with Si values between 2.99 and 3.13 apfu.
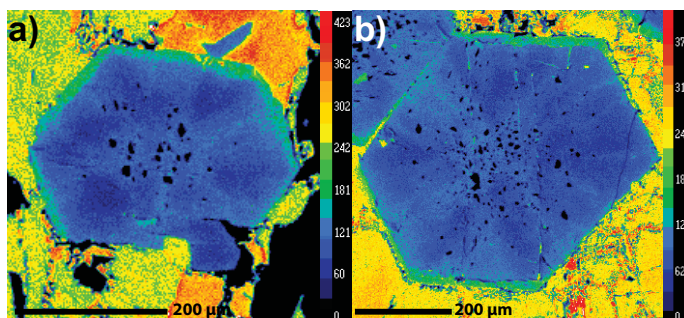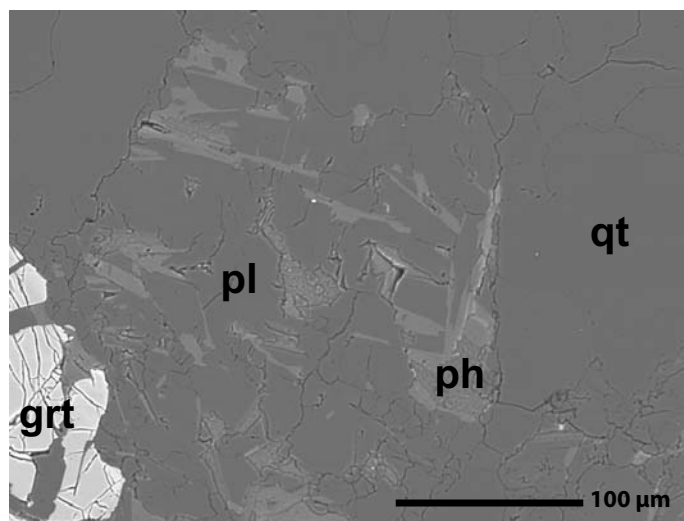
Other Phases

Representative compositions of biotite, plagioclase, K-feldspar and epidote are presented in Table DR-4. Biotite that has completely replaced phengite in the matrix of eclogite is relatively homogeneous (Si = 2.79–2.87 apfu, X_{Mg} [Mg/(Mg+Fe)] = 0.54–0.63, TiO_2 = 2.70–3.74 wt.%). Biotite in garnet has a similar X_{Mg} (0.53–0.68), but is richer in Si (2.97–3.07 apfu) and much lower in TiO_2 (0.14–0.16 wt.%) than matrix grains. Biotite in symplectites with plagioclase shows much wider compositional variations with respect to Si (2.66–3.27 apfu) and TiO_2 (0.86–3.69 wt.%), but displays a similar X_{Mg} (0.48–0.49). In metatonalite, biotite matrix and symplectite grains are homogeneous (Si = 2.75–2.80 apfu, X_{Mg} = 0.49–0.51, TiO_2 = 1.63–1.76 wt.%). Biotite in metasedimentary rocks has a range of Si (2.72–2.89 apfu) and X_{Mg} (0.48–0.52) similar to metatonalite biotite, but with a wider range in TiO_2 (1.20–2.31 wt.%). Plagioclase in eclogite is albite–oligoclase ($An_{2–22}$) in symplectites with clinopyroxene and where it is included in garnet. In symplectites with phengite, plagioclase is oligoclase ($An_{9–30}$). Plagioclase in metatonalite and metasedimentary rocks is also albite–oligoclase, ranging from $An_{2–26}$ and $An_{3–32}$, respectively. These ranges fall within the peristerite miscibility gap, and both albite and oligoclase occur as intergrowths in matrix grains within each sample. K-feldspar was identified in one sample as fine grains adjacent to plagioclase in the range $An_{0.5–3}$. Epidote is found in both eclogite and
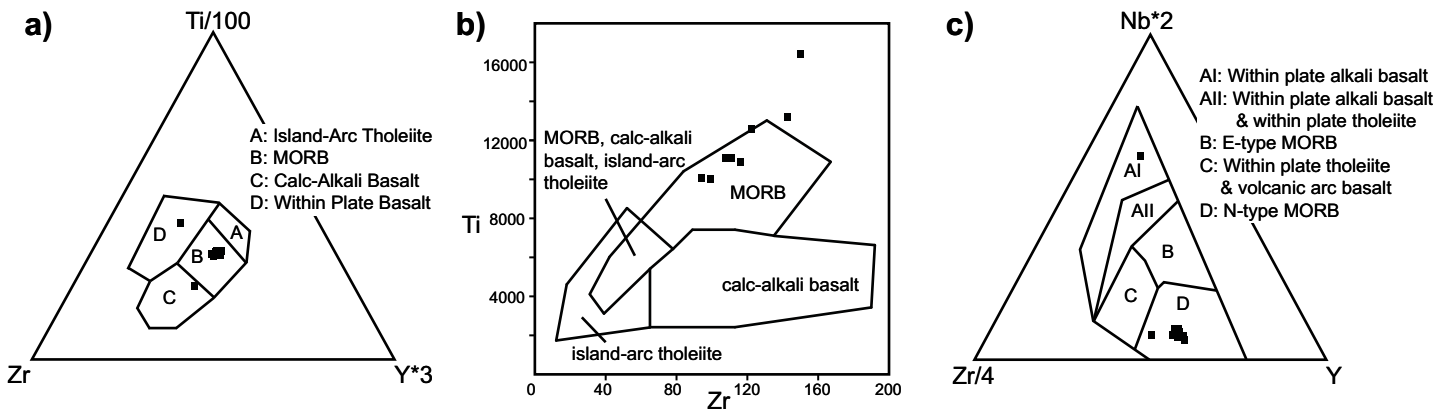
Figure 14. Trace element discrimination diagrams for eclogite to identify the protolith and its tectonic setting in the St. Cyr klippe. (a) and (b) trace element discrimination diagrams of Ti–Zr–Y and the Ti–Zr, respectively, from Pearce and Cann (1973). (c) Nb–Zr–Y plot from Meschede (1986). The protolith is primarily normal mid-oceanic ridge basalt (N-MORB).

metatonalite, and clinozoisite is present in metasedimentary rocks. In eclogite, the pistacite component $[Ca_2Al_2Fe^{3+}Si_3O_{12}(OH)]$ in epidote in the matrix and included in garnet lies between 23–35 mol% and 10–34 mol%, respectively. In metatonalite, epidote after plagioclase has a pistacite component of 20–29 mol%. Clinozoisite from one metasedimentary sample is 0.04 to 5 mol% in pistacite content.

GEOCHEMISTRY

Whole rock major and trace element concentrations for ten eclogite samples were analyzed by X-ray fluorescence and inductively coupled plasma mass spectrometry, respectively, at the GeoAnalytical Laboratory of Washington State University, Pullman, WA, following conventional procedures (Johnson et al. 1999). Bulk composition (Table DR-5) reveals that the eclogite is basaltic in composition. SiO_2 content is 45.2–51.1 wt.%, with TiO_2 = 1.7–2.7 wt.% and Na_2O = 2.5–4.0 wt.%. Trace element discrimination diagrams (Fig. 14) show that most of the St. Cyr eclogite samples fall in the mid-ocean ridge basalt (MORB) field of the Ti–Zr–Y and the Ti–Zr plot (Pearce and Cann 1973) and the normal type MORB (N-MORB) field in the Nb–Zr–Y plot (Meschede 1986). The primitive mantle trace element-normalized plot (Fig. 15) shows that the eclogite compositions broadly correlate with N-MORB (Sun and McDonough 1989).

ZIRCON U–PB GEOCHRONOLOGY AND TRACE ELEMENT GEOCHEMISTRY OF METATONALITE

U–Pb dates of zircon from four metatonalite samples were obtained in an effort to determine the age of the protolith and high-pressure metamorphism. The four samples were chosen based on their close proximity to eclogite lenses. Cathodoluminescence (CL) images of zircon (Fig. 16) guided the choice of analytical spots. U–Pb data is presented in Tables DR-6, DR-8 and Figure 17, and trace element data is in Table DR-7 and Figure 18.

Analytical Methods

Zircon grains were separated from 1–3 kg samples by standard physical separation techniques and mounted in 2.54 cm epoxy rounds, which were polished to expose grain interiors. CL, transmitted light and reflected light images were used to characterize zircon domains, identify internal growth zones and
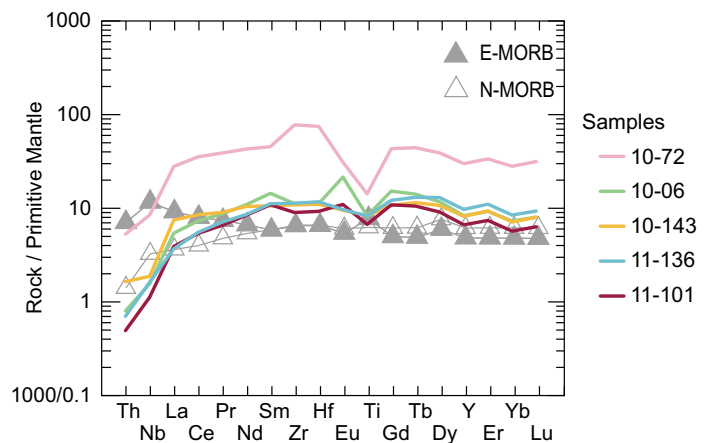

Figure 15. Primitive mantle-normalized plot based on Sun and McDonough (1989) for eclogite and retrogressed eclogite in the St. Cyr klippe. Normal mid-ocean ridge basalt (N-MORB) and enriched mid-ocean ridge basalt (E-MORB) are shown for reference (Sun and McDonough 1989).

select spot locations for analysis (Fig. 16).

U–Th–Pb isotopes and trace element data were measured on three samples (11-94, 11-114, and 12-17) using the sensitive high-resolution ion microprobe-reverse geometry (SHRIMP–RG) mass spectrometer at the U.S. Geological Survey – Stanford University ion probe facility, Stanford, California. Calibration of U was based on zircon standard Madagascar Green (MAD; 4196 ppm U; Barth and Wooden 2010). Isotopic ratios were calibrated by replicate analysis of zircon standard R33 (421 Ma, Black et al. 2004; Mattinson 2010), which was rerun after every fourth analysis. The analytical routine followed Barth and Wooden (2006, 2010). Uncertainties in the isotopic ratios are reported at the 1σ level. Ages are assigned based on the weighted mean of $^{206}Pb/^{238}U$ ages corrected for common Pb using the ^{207}Pb correction method (Williams 1998). Uncertainties in the weighted mean ages discussed below are reported at the 95% confidence level. The weighted mean ages are equivalent within uncertainty to concordia ages calculated in Squid 1.13 (Ludwig 2005). Age calculations and Tera-Wasserburg diagrams (Fig. 17) were generated with the Isoplot 3 program of Ludwig (2003).

Trace element data for Y, REE and Hf were collected simultaneously with the U, Th and Pb analyses. The following peaks were measured: ^{89}Y, ^{139}La, ^{140}Ce, ^{146}Nd, ^{147}Sm, ^{153}Eu,
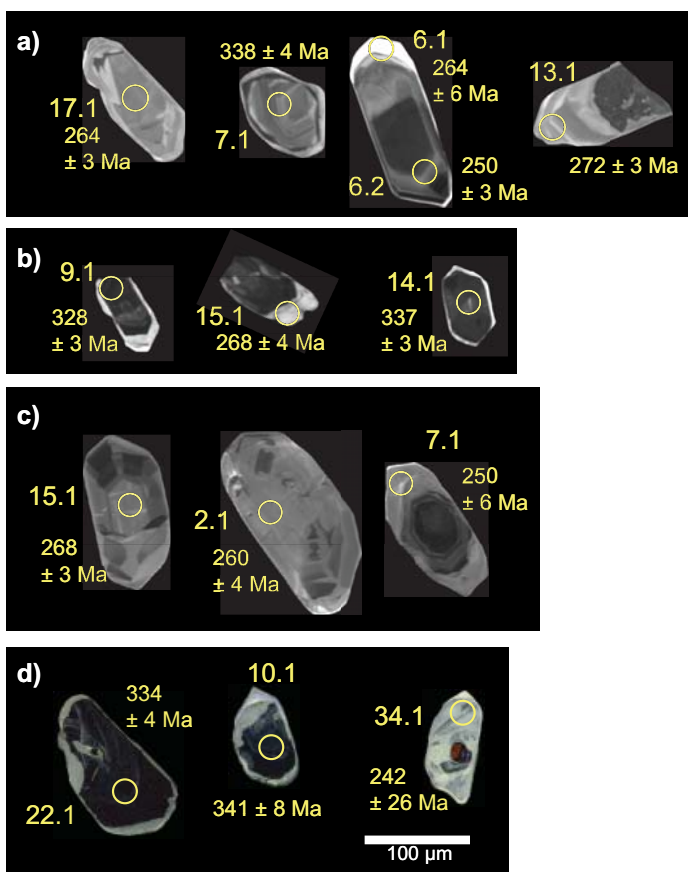
Figure 16. Representative cathodoluminescence (CL) images of zircon in (a) 11-94, (b) 11-114, and (c) 12-17. (d) Representative color CL images of zircon in 11-98. Ellipses indicate SHRIMP-RG U–Pb and trace element analysis spots labeled by grain and spot number.

$^{157}Gd^{16}O$, $^{163}Dy^{16}O$, $^{166}Er^{16}O$, $^{172}Yb^{16}O$, $^{90}Zr_2^{16}O$, $^{180}Hf^{16}O$, ^{206}Pb, $^{232}Th^{16}O$, $^{238}U^{16}O$. Data reduction of elemental concentrations used zircon standards CZ3 and MAD (Mazdab and Wooden 2006; Mazdab 2009). Chondrite-normalized REE plots (Fig. 18) use the chondrite REE abundances of Anders and Grevesse (1989) multiplied by a factor of 1.36 (Korotev 1996). Chondrite-normalized values for Pr were calculated by interpolation ($Pr_{(N)} = La_{(N)}^{0.33} \times Nd_{(N)}^{0.67}$). Eu and Ce anomalies are based on $Eu_{(N)}/Eu^*$ and $Ce_{(N)}/Ce^*$ with Eu^* and Ce^* calculated as geometric means (e.g. $Eu^* = (Sm_{(N)} \times Gd_{(N)})^{0.5}$).

The fourth metatonalite sample (11-98) was analyzed by laser ablation inductively coupled mass spectrometry (LA–ICP–MS) at the University of Arizona LaserChron Center using a spot size of 30 µm. Analytical procedures followed Gehrels et al. (2006, 2008). Common Pb corrections were made using ^{204}Hg-corrected ^{204}Pb measurements for each analysis, and initial Pb compositions of Stacey and Kramers (1975). U and Th concentrations and Pb/U fractionation were calibrated against the Arizona Laserchron Center Sri Lanka (SL) zircon standard (563.5 ± 3.2 Ma; ~518 ppm U and 68 ppm Th; Gehrels et al. 2008). Standards were analyzed at the beginning, end, and after every 5 grains for the primary standard (SL) and after every 15 grains for the secondary standard (R33).

Metatonalite Sample 11-94
Sample 11-94 was collected several metres away from an approximately two metre diameter eclogite boudin in the

south-central part of the field area (Fig. 3). It is a medium-grained, moderately foliated metatonalite schist, with an estimated mode of 50% quartz, 30% plagioclase, 15% phengite and 5% biotite. Accessory phases include epidote, apatite, garnet and titanite. Plagioclase is replaced by very fine grains of phengite, epidote and K-feldspar. Isolated garnet is replaced by chlorite along rims and fractures. Phengite is partially replaced by biotite, which is in turn overprinted by chlorite.

Zircon in sample 11-94 is elongate, euhedral to subrounded, with complex cores and rims (Fig. 16). Some oscillatory zoned, subrounded cores are surrounded by CL-dark mantles and homogeneous CL-light grey rims (e.g. grain 7 in Fig. 16a). Other euhedral cores are zoned but appear patchy and are overgrown by thicker coarsely-zoned rims (Fig. 16a, grain 17). Grains with round, CL-dark, mottled cores display coarsely-zoned rims that are moderately luminescent in CL (Fig. 16a, grain 13). The analyzed cores and rims can be divided into three populations defined by variations in trace element composition. Eight core analyses, with ^{207}Pb-corrected $^{206}Pb/^{238}U$ ages ranging from 303 to 349 Ma, are characterized by steep HREE (Yb/Gd = 6–41), ΣREE = 308–2136, negative Eu and positive Ce anomalies (Eu/Eu* = 0.2–0.6 and Ce/Ce* = 2–35) and Th/U ratios of 0.1–0.3, all typical of igneous zircon (Hoskin and Schaltegger 2003). Two cores have elevated light REE (LREE; Fig. 18a) indicating probable modification of the original trace element signature. The remaining six cores give a weighted mean $^{206}Pb/^{238}U$ age of 331 ± 4 Ma (mean square weighted deviation, MSWD = 1.5), which we interpret as the igneous crystallization age. Eight core and rim analyses show a strong depletion of ΣREE (32–61), a pronounced flattening of the HREE pattern (Yb/Gd = 2–13), no negative Eu anomaly (Fig. 18a) and Th/U ratios ranging from 0.004 to 0.01. These are all characteristics consistent with the growth or recrystallization of zircon during high-pressure metamorphism in the presence of garnet (Rubatto 2002; Rubatto and Hermann 2007). The ^{207}Pb-corrected $^{206}Pb/^{238}U$ ages from zircon displaying a flat HREE pattern range from 249 to 284 Ma. Assuming the older two analyses reflect mixing with protolith zircon and the two younger ages reflect Pb-loss or continued recrystallization, the remaining grains with flat HREE patterns and low REE abundance give a weighted mean $^{206}Pb/^{238}U$ age of 268 ± 4 Ma (MSWD = 1.1). The final group includes five oscillatory zoned or patchy cores and three metamorphic rims that have elevated ΣREE (129–837) and steep HREE (Yb/Gd = 37–822) compared to grains with flat HREE signatures, but similarly low Th/U (0.002–0.003) values and no negative Eu anomaly (Fig. 18a). Metamorphic ^{207}Pb-corrected $^{206}Pb/^{238}U$ ages from zircon with steep HREE range from 259 to 271 Ma. Assuming the youngest analysis reflects Pb-loss, seven analyses from zircon with steep HREE give a weighted mean $^{206}Pb/^{238}U$ age of 266 ± 3 Ma (MSWD = 1.7). The age difference between metamorphic zircon with flat versus steep HREE patterns is not distinguishable. Pooling ages from both groups of metamorphic zircon gives a weighted mean $^{206}Pb/^{238}U$ age of 266 ± 3 Ma (MSWD = 1.4), which is interpreted as the best estimate for high-pressure metamorphism (Fig. 17a). Grains with flat HREE patterns are inferred to be slightly older than zircon with steep patterns based on textural evidence: the core of grain 6 has a flat HREE pattern whereas the rim displays a steep HREE pattern (Fig. 16a). The change in REE abundance
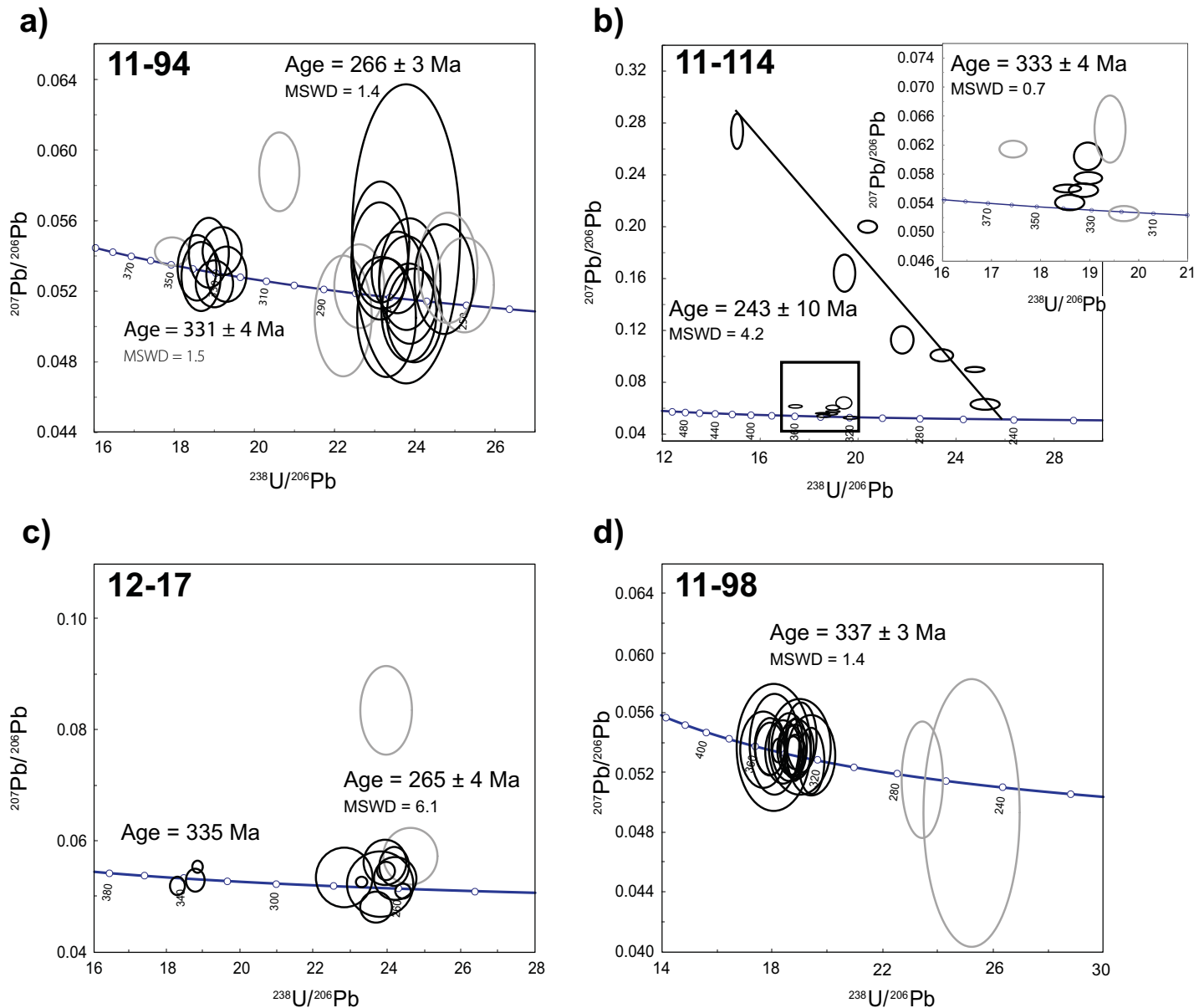
Figure 17. Terra–Wasserburg plots of SHRIMP-RG U–Pb data from metatonalite samples (a) 11-94, (b) 11-114, (c) 12-17 and (d) 11-98. Data are 1σ error ellipses uncorrected for common Pb. Black ellipses are used in calculating concordia ages. Errors are reported at the 95% confidence level. (a) Weighted mean ages were calculated for 11-94. (b) A concordia age was calculated for the crystallization age of sample 11-114 and an intercept age of 243 ± 10 Ma was calculated for the metamorphic age. (c) A weighted mean was calculated for the crystallization and high-pressure metamorphic ages of 12-17. (d) The igneous crystallization age is interpreted to be 337 ± 3 Ma.

and HREE pattern is interpreted to reflect the breakdown of garnet during continued high-pressure metamorphism, but additional analysis is required to confirm this hypothesis.

Metatonalite Sample 11-114

Sample 11-114 was collected adjacent to an eclogite boudin in the south-central part of the field area (Fig. 3). It is a fine- to medium-grained, metatonalite schist composed of approximately 50% quartz, 20% plagioclase and 30% white mica; titanite and apatite are accessory phases. Plagioclase is replaced by fine grains of white mica. Unlike sample 11-94, this sample lacks garnet altogether. Retrograde microstructures include white mica replaced by biotite, and biotite replaced by chlorite. A well-developed schistosity is defined by the planar alignment of phyllosilicate grains.

Zircon in sample 11-114 preserves CL-dark cores with faint oscillatory zoning overgrown by CL-bright rims (Fig. 16b). Seven cores with ^{207}Pb-corrected ^{206}Pb/^{238}U ages spanning 303–338 Ma have characteristic igneous trace element patterns, including steep HREE patterns (Yb/Gd = 7-17), ΣREE = 724–1170, Th/U = 0.1–0.4, a positive Ce anomaly (Ce/Ce* = 3–22) and a modestly developed negative Eu anomaly (Eu/Eu* = 0.3; Fig. 18b). Five of those cores give a ^{206}Pb/^{238}U concordia age of 333 ± 4 Ma (MSWD = 0.7; Fig. 17b), although two cores have elevated LREE patterns (Fig. 16b), indicating possible partial resetting of the protolith U–Pb systematics. The age of CL-dark cores is interpreted as the age of the protolith, which is within error of the 331 ± 4 Ma age of oscillatory zoned and patchy cores in sample 11-94.

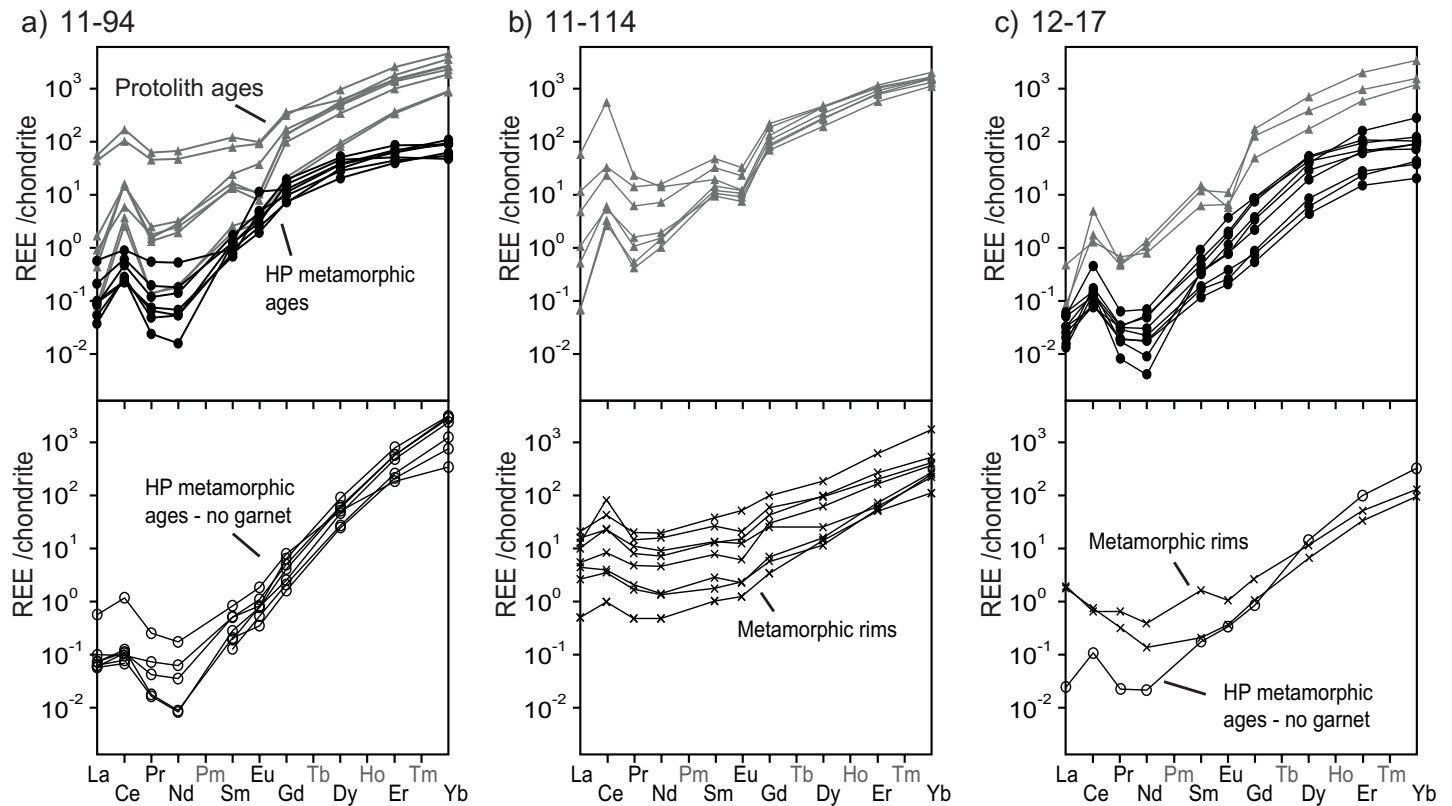Cl-bright rims give ^{207}Pb-corrected ^{206}Pb/^{238}U ages between

Figure 18. Chondrite-normalized REE patterns for different age populations of zircon grains from metatonalite samples (a) 11-94, (b) 11-114, and (c) 12-17. Normalization uses chondrite abundances from Anders and Grevesse (1989) multiplied by 1.36 (Korotev 1996). Ages are divided into igneous crystallization ages (light grey triangles) and metamorphic ages (open black circles – high-pressure with steep HREE patterns; filled black circles – high-pressure with flat HREE patterns; black crosses – metamorphic with high LREEs).

356–243 Ma, overlapping in part with the ages of the cores. The rims have variable trace element signatures with generally more elevated ΣREE (49–832), steeper HREE (Yd/Gd = 6–39) patterns and Th/U ratios ranging from igneous core values of 0.3 to 0.004 (Fig. 18b). In addition, the rims trend toward smaller or no negative Eu anomalies and depressed Ce anomalies (Fig. 18b). The steep HREE patterns for metamorphic zircon are interpreted to reflect the lack of garnet in the sample. Three-dimensional linear regression of the seven youngest rim ages with relatively high common Pb values defines a lower intercept of 243 ± 10 Ma (MSWD = 4.2). Assuming high-pressure metamorphism at 266 ± 3 Ma based on sample 11-94, the relatively high MSWD of 4.2 for regression of the rim analyses is interpreted to reflect dispersion in the analyses resulting from a complex history of post-high-pressure metamorphic overgrowths or disturbance of U–Pb systematics of the protolith zircon during exhumation.

Metatonalite Sample 12-17

Sample 12-17 was collected directly above a contact with metasedimentary schist in the central portion of the field area (Fig. 3). This fine-grained metatonalite schist contains about 60% plagioclase, 15% quartz, 10% epidote, 9% biotite and 6% white mica, with garnet, titanite and apatite as accessory phases. Plagioclase is replaced by small white mica grains and lobate symplectites of epidote. Retrograde features include white mica replaced by biotite, and biotite replaced by chlorite. A moderately developed schistosity is defined by the planar alignment of phyllosilicate grains.

Zircon in sample 12-17 is elongate and euhedral or sub-rounded, and preserves complexly zoned dark- to medium-grey cores surrounded by CL-bright rims (Fig. 16c). Zircon cores are dark, and oscillatory zoned or homogeneous (grain 7.1 in Fig. 16c), while others are mottled or patchy (Fig. 16c, grain 2.1). Still other cores are sector-zoned, a common zoning pattern preserved in zircon grown in the eclogite facies (Fig. 16c, grain 15.1; Corfu et al. 2003). Analysis of three oscillatory zoned cores give ^{207}Pb-corrected ^{206}Pb/^{238}U ages ranging from 332 to 343 Ma. Trace element patterns are characterized by steep HREE (Yb/Gd = 12–23), high ΣREE = 3141–10,278, negative Eu and positive Ce anomalies (Eu/Eu* = 0.1–0.3 and Ce/Ce* = 2–33) and Th/U ratios typical of igneous zircon ranging from 0.2–0.4. The three cores give a weighted mean ^{206}Pb/^{238}U age of 335 ± 14 Ma (MSWD = 6.9). The U–Pb ages and systematics, as well as the trace element signature defined by the three core analyses, are consistent with the protolith ages and signatures determined for the other samples. Accordingly, a protolith age of ca. 335 Ma is inferred for metatonalite sample 12-17.

Ten mottled, patchy, or sector-zoned cores give ^{207}Pb-corrected ^{206}Pb/^{238}U ages ranging from 255 to 276 Ma. These cores display depleted ΣREE values (94–697), Th/U values in the range of 0.001–0.02 and lack a negative Eu anomaly (Eu/Eu* = 0.001–0.02) as is typical of high-pressure metamorphic zircon. The middle (M)REE patterns are relatively steep, but most analyses show flattening of the HREE patterns (Yb/Gd = 8–454; Fig. 18c). The ten zircon cores give a weighted mean ^{206}Pb/^{238}U age of 265 ± 4 Ma (MSWD = 6.1).

The large spread in ages and high MSWD indicate the calculated age incorporates multiple unresolved components. Two CL-bright rims (grain 7.1 in Fig. 16c) gave the youngest ages and record low Th/U (0.01–0.004), depleted ΣREE values (185–277), steep HREE patterns (Yb/Gd = 49–96) and minor negative Eu anomalies (0.5–0.8). The relatively high common Pb and elevated LREE patterns (Fig. 18c) suggest these analyses may be affected by alteration and the ages were therefore excluded from calculation of the weighted mean ^{206}Pb/^{238}U age. Exclusion of additional analyses to reduce the observed MSWD of 6.1 is possible. For example, exclusion of analyses 9.1 and 14.1 based on the interpretation that the slightly older ages reflect mixed protolith and metamorphic domains yields a revised age of 262 ± 2 Ma with a more reasonable MSWD = 1.4. There is, however, no evidence from the CL images or trace element chemistry that justify this exclusion. Alternatively, younger analyses may be excluded assuming they represent post-high-pressure metamorphism or Pb-loss in order to bring the MSWD to acceptable levels. In the absence of clear textural or chemical evidence for defining subgroups of data, the age of 264 ± 5 Ma, which is consistent with the age of high-pressure metamorphism determined for sample 11-94, is viewed as the best estimate for eclogite-facies metamorphism for this sample. The range in ages and consequent high MSWD are attributed to unresolved complexities in the zircon systematics.

Metatonalite Sample 11-98

Sample 11-98 is a fine-grained metatonalite schist collected several metres away from a large eclogite boudin in the south-central part of the field area (Fig. 3). The sample is composed of ~ 40% quartz, 35% plagioclase, 10% biotite, 10% epidote and 5% white mica; garnet, ilmenite titanite and apatite are accessory phases. Plagioclase is replaced by fine grains of white mica and epidote. White mica is replaced by biotite, biotite is replaced by chlorite, and a well-developed schistosity is defined by the planar alignment of phyllosilicate grains.

Zircon in 11-98 is elongate and euhedral, and preserves dark- to medium-grey, oscillatory zoned cores surrounded by CL-bright rims (Fig. 16d). The majority of analyses give ^{206}Pb/^{238}U ages ranging from 323 to 365 Ma with two analyses yielding younger ages of 251 and 269 Ma (Fig. 17d). The young ages are interpreted to record Pb-loss, growth or recrystallization associated with metamorphism as observed in samples 11-94, 11-114 and 12-17. The 25 older zircon grains give a weighted mean ^{206}Pb/^{238}U age of 337 ± 3 Ma (MSWD = 1.4), which is similar to the igneous crystallization ages of the other three samples and interpreted as the protolith age for this sample.

DISCUSSION

The St. Cyr klippe is a complex collection of thrust slices that records contrasting geologic histories. The imbricate stack includes a slice of greenschist-facies oceanic-like crust and serpentinized mantle, and thrust sheets of different units of the Yukon–Tanana terrane. Two imbricate panels of amphibolite-facies quartzofeldspathic schist form part of the Snowcap assemblage, which constitutes the basal substrate to the arc assemblages (e.g. Colpron et al. 2006a). Snowcap assemblage rocks are thrust on top of at least two slices of eclogite-bearing quartzofeldspathic schist that are dominated by Yukon–

Tanana arc material. Igneous crystallization ages for metatonalite samples (337 to 331 Ma) fall within the Little Salmon Cycle (as defined by Piercey et al. 2006) of the Klinkit phase of Yukon–Tanana arc activity (342 to 314 Ma; Nelson et al. 2006 and references therein). Felsic metaigneous and metavolcanic rocks of similar age are found in the Yukon–Tanana terrane in the Fortymile River assemblage in eastern Alaska, the Tatlmain Plutonic Suite and Little Salmon Formation in the Glenlyon area of central Yukon, and the Ram Creek and Big Salmon complexes in the Wolf Lake–Jennings River area of southern Yukon–northern British Columbia (Nelson and Friedman 2004; Colpron et al. 2006b; Dusel-Bacon et al. 2006; Roots et al. 2006).

Whole-rock composition of eclogite indicates that its protolith was N-MORB-like tholeiitic basalt. Primitive basalt is found throughout the Yukon-Tanana arc, from initial arc formation in the Mid- to Late Devonian through the Late Permian (Colpron et al. 2006a; Nelson et al. 2006). In addition, the penetrative fabrics shared by eclogite and the host rocks and widespread high-pressure metamorphism contrast with the low-grade, weakly deformed oceanic pelagic sedimentary rocks that are common to the Slide Mountain terrane (Wheeler et al. 1991; Colpron et al. 2006a; Piercey et al. 2012). Therefore, we conclude that the eclogite is derived from the Yukon–Tanana terrane, rather than the Slide Mountain terrane.

The eclogite-bearing quartzofeldspathic rocks at St. Cyr record evidence of high-pressure metamorphism consistent with that of other Permian high-pressure rocks in the Yukon–Tanana terrane (e.g. Erdmer et al. 1998). Trace element signatures of metamorphic zircon in metatonalite samples 11-94 and 12-17 indicate their formation under garnet-present, plagioclase-absent pressure–temperature conditions, consistent with eclogite-facies paragenesis. These zircon grains record a high-pressure metamorphic age of 266 ± 3 to 265 ± 4 Ma, which agrees with the SIMS ages (271–267 Ma) determined for eclogite (Petrie 2014) and the U–Pb TIMS zircon age of 266 ± 0.6 Ma derived from eclogite (Fallas et al. 1998). These dates are also within error of a U–Pb zircon age interpreted to record the high-pressure metamorphism of eclogite at Last Peak (269 ± 2 Ma; Creaser et al. 1997), and corroborate other Permian eclogite-facies assemblages attributed to the Yukon–Tanana terrane.

The St. Cyr klippe is significant in that it represents a glimpse into Late Permian high-pressure metamorphism in the Yukon–Tanana terrane. Taken as a whole, the Yukon–Tanana terrane is a complex polymetamorphic terrane, recording multiple ages and pressure–temperature ranges of peak metamorphism. For example, in the Stewart River area, titanite and monazite ages suggest that Yukon-Tanana arc and Snowcap assemblage rocks were metamorphosed during deformation at relatively low-pressure conditions between 365 and 350 Ma and at medium-pressure conditions at ~ 265 Ma (Berman et al. 2007). These rocks were further overprinted by regional Cretaceous plutonism and Jurassic–Cretaceous metamorphism during deformation and exhumation (Berman et al. 2007; Staples et al. 2013). In the St. Cyr area, the majority of ^{40}Ar/^{39}Ar muscovite cooling ages (Fallas et al. 1998) fall between 263 Ma and 235 Ma, further demonstrating that high-pressure rocks in the St. Cyr klippe escaped the regionally pervasive Jurassic and Cretaceous metamorphic overprint recorded in other

Yukon–Tanana terrane rocks.

Eclogite in the St. Cyr klippe is remarkably well preserved, and comparison of the petrological and chemical signatures to the three other eclogite localities suggests a genetic link. In the St. Cyr klippe, omphacite (Jd_{20-49}) and phengite (up to 3.67 Si apfu) compositions overlap with those of eclogite in Ross River, Faro and Last Peak (Erdmer 1987; Erdmer et al. 1998; Perchuk et al. 1999; Perchuk and Gerya 2005; Ghent and Erdmer 2011). Phengite in the host quartzofeldspathic schist contains values of Si between 3.20 and 3.48, which is slightly higher than the Si content of phengite in garnet–mica schist at Last Peak (3.20 to 3.38 Si apfu; Hansen 1992). Eclogite at Ross River is hosted by quartzofeldspathic garnet–mica- and glaucophane-bearing schist (Erdmer 1987; Erdmer and Armstrong 1989; Ghent and Erdmer 2011), at Faro by glaucophane-bearing and garnet–mica schist that contains phengite (Perchuk et al. 1999; Perchuk and Gerya 2005), and at Last Peak, by hornblende, biotite, and phengite-bearing schist (Erdmer and Helmstaedt 1983; Erdmer et al. 1998). These rocks bear a resemblance to the host rocks in the St. Cyr klippe, although the amphibole is less sodic at St. Cyr. At each of the three other localities, the peak eclogite-facies assemblage is omphacite + garnet + quartz, which is the dominant peak assemblage at St. Cyr (Creaser et al. 1997; Erdmer et al. 1998). Phengite is confirmed in eclogite from Ross River and Faro (Erdmer 1987; Perchuk et al. 1999). Like eclogite at St. Cyr, during the transition from eclogite to garnet amphibolite, omphacite was replaced primarily by calcic amphibole, such as pargasite, and albitic plagioclase (Erdmer and Helmstaedt 1983; Erdmer 1987; Creaser et al. 1997; Perchuk et al. 1999). Geochemically, the MORB signature recorded in the major and trace element geochemistry of St. Cyr eclogite is consistent with the geochemical signatures of eclogite at all three localities (Erdmer and Helmstaedt 1983; Creaser et al. 1999; Pigage 2004; Ghent and Erdmer 2011). Thus, the Permian eclogites in the Yukon–Tanana terrane are not isolated occurrences, but form part of a regional high-pressure lithotectonic assemblage.

When eclogite was first identified in the St. Cyr area, the high-pressure mafic rocks were assumed to have formed at depth and returned to the surface within a tectonic mélange (e.g. Erdmer 1987). The results of our investigation show that the basaltic protolith of the eclogite existed within the quartzofeldspathic host rocks of the Yukon–Tanana terrane prior to subduction, and experienced the same metamorphic history. Thus, the high-pressure assemblage in the St. Cyr klippe represents slices of coherent continental arc crust subducted to high-pressure conditions in Permian time. The idea of emplacement of exotic slivers versus metamorphism *in situ* of high-pressure rocks was something of a controversy in high-pressure and ultrahigh-pressure (UHP) terranes, such as the Western Gneiss Region in Norway and the Dabie-Sulu UHP terrane in China (e.g. Smith 1984; Wang and Liou 1991). The argument was largely due to the rare preservation of the pre- versus post-metamorphic field relationships between eclogite and the host rocks, as well as retrograde overprinting of the host rocks that erased the evidence of UHP metamorphism (Andersen et al. 1991; Zhang et al. 1995). Numerous studies on the eclogite-bearing host rocks in these localities have shown that those rocks have in fact been subjected to coeval high-

pressure and UHP metamorphism (Wang and Liou 1991; Zhang et al. 1995; Wain 1997; Carswell et al. 2003; Liu et al. 2005; Butler et al. 2013), and hence they represent coherent slices of continental crust. Eclogite in the St. Cyr klippe also formed *in situ* with the enveloping high-pressure, Yukon–Tanana derived schist, and thus constitutes coherent slices of Yukon–Tanana terrane arc-derived rocks.

CONCLUSIONS

The St. Cyr klippe consists of variably metamorphosed and deformed, structurally imbricated units of Yukon–Tanana continental arc crust and ultramafic–mafic rocks of possible oceanic affinity. However, the absence of any other rocks typical of the Slide Mountain terrane argues that these rocks did not form part of this oceanic assemblage. Quartzofeldspathic schist derived from the Yukon–Tanana terrane host sub-metre to hundreds of metres scale lenses of well-preserved eclogite and retrogressed eclogite. The presence of phengite and high-pressure zircon in quartzofeldspathic schist shows that eclogite was metamorphosed *in situ* with its host rock during the Late Permian. This confirms that the eclogite-bearing unit consists of slices of coherent arc crust, and that the eclogite is not part of a tectonic mélange. The petrological, geochemical, geochronological, and structural relationships between eclogite and the host rocks in the St. Cyr klippe are shared with similar high-pressure assemblages found in the Yukon–Tanana terrane at Faro, Ross River and Last Peak. These mutual relationships suggest that Permian high-pressure assemblages form part of a larger high-pressure lithotectonic assemblage within the Yukon–Tanana terrane.

REFERENCES
Anders, E., and Grevesse, N., 1989, Abundances of the elements: Meteoritic and solar: Geochimica et Cosmochimica Acta, v. 53, p. 197–214, http://dx.doi.org/10.1016/0016-7037(89)90286-X.

Andersen, T.B., Jamtveit, B., Dewey, J.F., and Swensson, E., 1991, Subduction and eduction of continental crust: major mechanisms during continent-continent collision and orogenic extensional collapse, a model based on the south Norwegian Caledonides: Terra Nova, v. 3, p. 303–310, http://dx.doi.org/10.1111/j.1365-3121.1991.tb00148.x.

Armbruster, T., Bonazzi, P., Akasaka, M., Bermanec, V., Chopin, C., Gieré, R., Heuss-Assbichler, S., Liebscher, A., Menchetti, S., Pan, Y., and Pasero, M., 2006, Recommended nomenclature of epidote-group minerals: European Journal of Mineralogy, v. 18, p. 551–567, http://dx.doi.org/10.1127/0935-1221/2006/0018-0551.

Barth, A.P., and Wooden, J.L., 2006, Timing of magmatism following initial convergence at a passive margin, southwestern U.S. Cordillera, and ages of lower crustal magma sources: The Journal of Geology, v. 114, p. 231–245, http://dx.doi.org/10.1086/499573.

Barth, A.P., and Wooden, J.L., 2010, Coupled elemental and isotopic analyses of polygenetic zircons from granitic rocks by ion microprobe, with implications for melt evolution and the sources of granitic magmas: Chemical Geology, v.

277, p. 149–159, http://dx.doi.org/10.1016/j.chemgeo.2010.07.017.

Berman, R.G., Ryan, J.J., Gordey, S.P., and Villeneuve, M., 2007, Permian to Cretaceous polymetamorphic evolution of the Stewart River region, Yukon-Tanana terrane, Yukon, Canada: *P-T* evolution linked with *in situ* SHRIMP monazite geochronology: Journal of Metamorphic Geology, v. 25, p. 803–827, http://dx.doi.org/10.1111/j.1525-1314.2007.00729.x.

Black, L.P., Kamo, S.L., Allen, C.M., Davis, D.W., Aleinikoff, J.N., Valley, J.W., Mundil, R., Campbell, I.H., Korsch, R.J., Williams, I.S., and Foudoulis, C., 2004, Improved $^{206}Pb/^{238}U$ microprobe geochronology by the monitoring of a trace-element-related matrix effect; SHRIMP, ID-TIMS, ELA-ICP-MS and oxygen isotope documentation for a series of zircon standards: Chemical Geology, v. 205, p. 115–140, http://dx.doi.org/10.1016/j.chemgeo.2004.01.003.

Butler, J.P., Jamieson, R.A, Steenkamp, H.M, and Robinson, P., 2013, Discovery of coesite– eclogite from the Nordøyane UHP domain, Western Gneiss Region, Norway: field relations, metamorphic history, and tectonic significance: Journal of Metamorphic Geology, v. 31, p. 147–163, http://dx.doi.org/10.1111/jmg.12004.

Carswell, D.A., Brueckner, H.K., Cuthbert, S.J., Mehta, K., and O'Brien, P.J., 2003, The timing of stabilisation and the exhumation rate for ultra-high pressure rocks in the Western Gneiss Region of Norway: Journal of Metamorphic Geology, v. 21, p. 601–612, http://dx.doi.org/10.1046/j.1525-1314.2003.00467.x.

Coleman, R.G., Lee, D.E., Beatty, L.B., and Brannock, W.W., 1965, Eclogites and eclogites: Their differences and similarities: Geological Society of America Bulletin, v. 76, p. 483–508, http://dx.doi.org/10.1130/0016-7606(1965)76[483:EAETDA]2.0.CO;2.

Colpron, M., 2006, Tectonic assemblage map of Yukon-Tanana and related terranes in Yukon and northern British Columbia: Yukon Geologic Survey, Open File 2006–1, scale: 1:1,000,000.

Colpron, M., Nelson, J.L., and Murphy, D.C., 2006a, A tectonostratigraphic framework for the pericratonic terranes of the northern Canadian Cordillera, *in* Colpron, M., and Nelson, J.L., *eds.*, Paleozoic Evolution and Metallogeny of Pericratonic Terranes at the Ancient Pacific Margin of North America, Canadian and Alaskan Cordillera: Geological Association of Canada, Special Paper 45, p. 1–23.

Colpron, M., Mortensen, J.K., Gehrels, G.E., and Villeneuve, M., 2006b, Basement complex, Carboniferous magmatism and Paleozoic deformation in Yukon-Tanana terrane of central Yukon: Field, geochemical and geochronological constraints from Glenlyon map area, *in* Colpron, M., and Nelson, J.L., *eds.*, Paleozoic Evolution and Metallogeny of Pericratonic Terranes at the Ancient Pacific Margin of North America, Canadian and Alaskan Cordillera: Geological Association of Canada, Special Paper 45, p. 131–151.

Colpron, M., Nelson, J.L., and Murphy, D.C., 2007, Northern Cordilleran terranes and their interactions through time: GSA Today, v. 17, p. 4–10, http://dx.doi.org/10.1130/GSAT01704-5A.1.

Corfu, F., Hanchar, J.M., Hoskin, P.W.O., and Kinny, P., 2003, Atlas of zircon textures, *in* Hanchar, J.M., and Hoskin, P.W.O., *eds.*, Zircon: Reviews in Mineralogy and Petrology: American Mineralogist, v. 53, p. 469–500, http://dx.doi.org/10.2113/0530469.

Creaser, R.A., Erdmer, P, Stevens, R.A., and Grant, S.L., 1997, Tectonic affinity of Nisutlin and Anvil assemblage strata from the Teslin tectonic zone, northern Canadian Cordillera: Constraints from neodymium isotope and geochemical evidence: Tectonics, v. 16, p. 107–121, http://dx.doi.org/10.1029/96TC03317.

Creaser, R.A., Goodwin-Bell, J-A.S., and Erdmer, P., 1999, Geochemical and Nd isotopic constraints for the origin of eclogite protoliths, northern Cordillera: implications for the Paleozoic tectonic evolution of the Yukon-Tanana terrane: Canadian Journal of Earth Sciences, v. 36, p. 1697–1709, http://dx.doi.org/10.1139/e99-070.

Devine, F., Carr, S.D., Murphy, D.C., Davis, W.J., Smith, S., and Villeneuve, M., 2006, Geochronological and geochemical constraints on the origin of the Klatsa metamorphic complex: Implications for Early Mississippian high-pressure metamorphism within Yukon-Tanana terrane, *in* Colpron, M., and Nelson, J.L., *eds.*, Paleozoic Evolution and Metallogeny of Pericratonic Terranes at the Ancient Pacific Margin of North America, Canadian and Alaskan Cordillera: Geological Association of Canada, Special Paper, 45, p. 107–130.

Dusel-Bacon, C., Hopkins, M.J., Mortensen, J.K., Dashevsky, S.S., Bressler, J.R., and Day, W.C., 2006, Paleozoic tectonic and metallogenic evolution of the pericratonic rocks of east-central Alaska and adjacent Yukon, *in* Colpron, M., and Nelson, J.L., *eds.*, Paleozoic Evolution and Metallogeny of Pericratonic Terranes at the Ancient Pacific Margin of North America, Canadian and Alaskan Cordillera: Geological Association of Canada, Special Paper 45, p. 25–74.

Erdmer, P., 1987, Blueschist and eclogite in mylonitic allochthons, Ross River and Watson Lake areas, southeastern Yukon: Canadian Journal of Earth Sciences, v. 24, p. 1439–1449, http://dx.doi.org/10.1139/e87-136.

Erdmer, P., 1992, Eclogitic rocks of the St. Cyr klippe, Yukon, and their tectonic significance: Canadian Journal of Earth Sciences, v. 29, p. 1296–1304, http://dx.doi.org/10.1139/e92-103.

Erdmer, P., and Armstrong, R.L., 1989, Permo–Triassic isotopic dates for blueschist, Ross River area, Yukon: Exploration and Geological Services Division, Yukon, Indian and Northern Affairs Canada, Yukon Geology, 2, p. 33–36.

Erdmer, P., and Helmstaedt, H., 1983, Eclogite from central Yukon: a record of subduction at the western margin of ancient North America: Canadian Journal of Earth Sciences, v. 20, p. 1389–1408, http://dx.doi.org/10.1139/e83-126.

Erdmer, P., Ghent, E.D., Archibald, D.A., and Stout, M.Z., 1998, Paleozoic and Mesozoic high-pressure metamorphism at the margin of ancestral North America in central Yukon: Geological Society of America Bulletin, v. 110, p. 615–629, http://dx.doi.org/10.1130/0016-7606(1998)110<0615:PAMHPM>2.3.CO;2.

Ernst, W.G., 2015, Franciscan geologic history constrained by tectonic/olistostromal high-grade metamafic blocks in the iconic Californian Mesozoic–Cenozoic accretionary complex: American Mineralogist, v. 100, p. 6–13, http://dx.doi.org/10.2138/am-2015-4850.

Evans, B.W., Hattori, K., and Baronnet, A., 2013, Serpentinite: What, Why, Where?: Elements, v. 9, p. 99–106, http://dx.doi.org/10.2113/gselements.9.2.99.

Fallas, K.M., 1997, Preliminary constraints on the structural and metamorphic evolution of the St. Cyr Klippe, south-central Yukon: LITHOPROBE Slave-Northern Cordillera Lithospheric Evolution (SNORCLE) Transect Meeting Report, March 7–9, 1997, University of Calgary, AB, v. 56, p. 90–95.

Fallas, K.M., Erdmer, P., Archibald, D.A., Heaman, L.M., and Creaser, R.A., 1998, The St. Cyr Klippe, south-central Yukon: an outlier of the teslin tectonic zone?: LITHOPROBE Slave- Northern Cordillera Lithospheric Evolution (SNORCLE) Transect Meeting Report, March 6–8, 1998, Simon Fraser University, BC, p. 131–138.

Fallas, K.M., Erdmer, P., Creaser, R.A., Archibald, D.A., and Heaman, L.M., 1999, New terrane interpretation for the St. Cyr Klippe, south-central Yukon: LITHOPROBE Slave-Northern Cordillera Lithospheric Evolution (SNORCLE) Transect Meeting Report, March 5–7, 1999, University of Calgary, AB, v. 69, p. 130–137.

Gehrels, G.E., Valencia, V., and Pullen, A., 2006, Detrital zircon geochronology by laser ablation multicollector ICPMS at the Arizona Laserchron Center; Geochronology: Emerging Opportunities, Paleontological Society Short Course: Paleontological Society Papers, v. 12, p. 67–76.

Gehrels, G.E., Valencia, V.A., and Ruiz, J., 2008, Enhanced precision, accuracy, efficiency and spatial resolution of U–Pb ages by laser ablation-multicollector-inductively coupled plasma- mass spectrometry: Geochemistry Geophysics Geosystems, v. 9, Q03017, http://dx.doi.org/10.1029/2007GC001805.

Ghent, E., and Erdmer, P., 2011, Very high-pressure epidote eclogite from Ross River area, Yukon, Canada, records deep subduction, *in* Dobrzhinetskaya, L.F., Faryad, S.W., Wallis, S., and Cuthbert, S., *eds.*, Ultrahigh-pressure Metamorphism: 25 Years after the Discovery of Coesite and Diamond: Elsevier, Burlington, MA, p. 441–457, http://dx.doi.org/10.1016/B978-0-12-385144-4.00013-8.

Gilotti, J.A., McClelland, W.C., Petrie, M.B., and van Staal, C., 2013, Interpreting subduction polarity from eclogite-bearing slices in accretionary orogens - a cautionary note from the Yukon-Tanana terrane (Abstract): Geological Society of America, Annual Meeting, 2013, Abstracts, p. 442.

Hansen, V.L., 1992, *P-T* evolution of the Teslin suture zone and Cassiar tectonites, Yukon, Canada: evidence for A- and B-type subduction: Journal of Metamorphic Geology, v. 10, p. 239–263, http://dx.doi.org/10.1111/j.1525-1314.1992.tb00081.x.

Hawthorne, F.C., Oberti, R., Harlow, G.E., Maresch, W.V., Martin, R.F., Schumacher, J.C., and Welch, M.D., 2012, Nomenclature of the amphibole supergroup: American Mineralogist, v. 97, p. 2031–2048, http://dx.doi.org/10.2138/am.2012.4276.

Hoskin, P.W.O., and Schaltegger, U., 2003, The composition of zircon and igneous and metamorphic petrogenesis, *in* Hanchar, J.M., and Hoskin, P.W.O., *eds.*, Zircon: Reviews in Mineralogy and Petrology, American Mineralogist, v. 53, p. 27–62, http://dx.doi.org/10.2113/0530027.

Isard, S.J., 2014, Origin of the Tower Peak unit, St. Cyr area, Canadian Cordillera: Unpublished MSc Thesis, University of Iowa, Iowa City, IA, 130 p.

Isard, S.J., and Gilotti, J.A., 2014, Geology and jade prospects of the northern St. Cyr klippe (NTS 105F/6), Yukon, *in* MacFarlane, K.E., Nordling, M.G., and Sack, P.J., *eds.*, Yukon Exploration and Geology: Yukon Geologic Survey, p. 69–77.

Johnson, D.M., Hooper, P.R., and Conrey, R.M., 1999, XRF Analysis of rocks and minerals for major and trace elements on a single low dilution Li-tetraborate fused bead: JCPDS- International Center for Diffraction Data, v. 41, p. 843–867.

Kleinschmidt, G., Heberer, B., and Läufer, A.L., 2008, Pre-Alpine sector-zoned garnets in the southeastern Alps: Zeitschrift der Deutschen Gesellschaft für Geowissenschaften, v. 159, p. 565–573, http://dx.doi.org/10.1127/1860-1804/2008/0159-0565.

Korotev, R.L., 1996, A self-consistent compilation of elemental concentration data

for 93 geochemical reference samples: Geostandards Newsletter, v. 20, p. 217–245, http://dx.doi.org/10.1111/j.1751-908X.1996.tb00185.x.

Liu, F., Liou, J.G., and Xu, Z., 2005, U–Pb SHRIMP ages recorded in the coesite-bearing zircon domains of paragneisses in the southwestern Sulu terrane, eastern China: New Interpretation: American Mineralogist, v. 90, p. 790–800, http://dx.doi.org/10.2138/am.2005.1677.

Ludwig, K.R., 2003, User's manual for Isoplot 3.00: a geochronological toolkit for Microsoft Excel: Berkeley Geochronology Center Special Publication, 4, p. 70.

Ludwig, K.R., 2005, Squid version 1.13b: A user's manual: Berkley Geochronology Center Special Publication, 2, p. 1–22.

Mattinson, J.M., 2010, Analysis of the relative decay constants of ^{235}U and ^{238}U by multi-step CA-TIMS measurements of closed-system natural zircon samples: Chemical Geology, v. 275, p. 186–198, http://dx.doi.org/10.1016/j.chemgeo.2010.05.007.

Mazdab, F.K., 2009, Characterization of flux grown trace-element-doped titanite using the high-mass-resolution ion microprobe (SHRIMP-RG): Canadian Mineralogist, v. 47, p. 813–831, http://dx.doi.org/10.3749/canmin.47.4.813.

Mazdab, F.K., and Wooden, J.L., 2006, Trace element analysis in zircon by ion microprobe (SHRIMP-RG): Technique and applications: Geochimica et Cosmochimica Acta, v. 70, A405, http://dx.doi.org/10.1016/j.gca.2006.06.817.

Meschede, M., 1986, A method of discriminating between different types of mid-ocean ridge basalts and continental tholeiites with the Nb-Zr-Y diagram: Chemical Geology, v. 56, p. 207– 218, http://dx.doi.org/10.1016/0009-2541(86)90004-5.

Monger, J.W.H., Price, R.A., and Tempelman-Kluit, D.J., 1982, Tectonic accretion and the origin of the two major metamorphic and plutonic welts in the Canadian Cordillera: Geology, v. 10, p. 70–75, http://dx.doi.org/10.1130/0091-7613(1982)10<70:TAATOO>2.0.CO;2.

Morimoto, N., 1989, Nomenclature of pyroxenes: Canadian Mineralogist, v. 27, p. 143–156, http://dx.doi.org/10.2465/minerj.14.198.

Mortensen, J.K., 1990, Geology and U–Pb geochronology of the Klondike District, west-central Yukon Territory: Canadian Journal of Earth Sciences, v. 27, p. 903–914, http://dx.doi.org/10.1139/e90-093.

Mortensen, J.K., 1992, Pre-Mid-Mesozoic tectonic evolution of the Yukon-Tanana terrane, Yukon and Alaska: Tectonics, v. 11, p. 836–853, http://dx.doi.org/10.1029/91TC01169.

Murphy, D.C., Mortensen, J.K., Piercey, S.J., Orchard, M.J., and Gehrels, G.E., 2006, Mid- Paleozoic to early Mesozoic tectonostratigraphic evolution of Yukon-Tanana and Slide Mountain terranes and affiliated overlap assemblages, Finlayson Lake massive sulphide district, southeastern Yukon, in Colpron, M., and Nelson, J.L., eds., Paleozoic Evolution and Metallogeny of Pericratonic Terranes at the Ancient Pacific Margin of North America, Canadian and Alaskan Cordillera: Geological Association of Canada, Special Paper, 45, p. 75–105.

Nelson, J.L., 1993, The Sylvester Allochthon: upper Paleozoic marginal-basin and island-arc terranes in northern British Columbia: Canadian Journal of Earth Sciences, v. 30, p. 631–643, http://dx.doi.org/10.1139/e93-048.

Nelson, J., and Friedman, R., 2004, Superimposed Quesnel (late Paleozoic–Jurassic) and Yukon- Tanana (Devonian–Mississippian) arc assemblages, Cassiar Mountains, northern British Columbia: Field, U–Pb, and igneous petrochemical evidence: Canadian Journal of Earth Sciences, v. 41, p. 1201–1235, http://dx.doi.org/10.1139/e04-028.

Nelson, J.L., Colpron, M., Piercey, S.J., Dusel-Bacon, C., Murphy, D.C., and Roots, C.F., 2006, Paleozoic tectonic and metallogenetic evolution of pericratonic terranes in Yukon, northern British Columbia and eastern Alaska, in Colpron, M., and Nelson, J.L., eds., Paleozoic Evolution and Metallogeny of Pericratonic Terranes at the Ancient Pacific Margin of North America, Canadian and Alaskan Cordillera: Geological Association of Canada, Special Paper 45, p. 323–360

Nelson, J.L., Colpron, M., and Israel, S., 2013, The Cordillera of British Columbia, Yukon, and Alaska: Tectonics and Metallogeny: Society of Economic Geologists Special Publication, v. 17, p. 53–109.

Pearce, J.A., and Cann, J.R., 1973, Tectonic setting of basic volcanic rocks determined using trace element analyses: Earth and Planetary Science Letters, v. 19, p. 290–300, http://dx.doi.org/10.1016/0012-821X(73)90129-5.

Perchuk, A.L., and Gerya, T.V., 2005, Dynamics of subsidence and exhumation of eclogites of the Yukon-Tanana terrane, (Canadian Cordilleras), according to petrological reconstructions and geodynamic modeling: Petrologiya, v. 13, p. 280–294.

Perchuk, A., Philippot, P., Erdmer, P., and Fialin, M., 1999, Rates of thermal equilibration at the onset of subduction deduced from diffusion modeling of eclogitic garnets, Yukon-Tanana terrane, Canada: Geology, v. 27, p. 531–534, http://dx.doi.org/10.1130/0091-7613(1999)027<0531:ROTEAT>2.3.CO;2.

Petrie, M.B., 2014, Evolution of eclogite facies metamorphism in the St. Cyr klippe, Yukon– Tanana terrane, Yukon, Canada: Unpublished Ph.D. Thesis, University of Iowa, Iowa City, IA, 168 p.

Piercey, S.J., and Colpron, M., 2009, Composition and provenance of the Snowcap assemblage, basement to the Yukon-Tanana terrane, northern Cordillera: Impli-

cations for Cordilleran crustal growth: Geosphere, v. 5, p. 439–464, http://dx.doi.org/10.1130/GES00505.1.

Piercey, S.J., Mortensen, J.K., Murphy, D.C., Paradis, S., and Creaser, R.A., 2002, Geochemistry and tectonic significance of alkalic mafic magmatism in the Yukon-Tanana terrane, Finlayson Lake region, Yukon: Canadian Journal of Earth Sciences, v. 39, p. 1729–1744, http://dx.doi.org/10.1139/e02-090.

Piercey, S.J., Nelson, J.L., Colpron, M., Dusel-Bacon, C., Simard, R.-L., and Roots, C.F., 2006, Paleozoic magmatism and crustal recycling along the ancient Pacific margin of North America, northern Cordillera, in Colpron, M., and Nelson, J.L., eds., Paleozoic Evolution and Metallogeny of Pericratonic Terranes at the Ancient Pacific Margin of North America, Canadian and Alaskan Cordillera: Geological Association of Canada, Special Paper 45, p. 281–322.

Piercey, S.J., Murphy, D.C., and Creaser, R.A., 2012, Lithosphere-asthenosphere mixing in a transform-dominated late Paleozoic backarc basin: Implications for northern Cordilleran crustal growth and assembly: Geosphere, v. 8, p. 716–739, http://dx.doi.org/10.1130/GES00757.1.

Pigage, L.C., 2004, Bedrock geology compilation of the Anvil District (parts of NTS 105K/2, 3, 5, 6, 7 and 11), central Yukon: Yukon Geological Survey Bulletin 15, p. 103.

Roots, C.F., Nelson, J.L., Simard, R.-L., and Harms, T.A., 2006, Continental fragments, mid- Paleozoic arcs and overlapping late Paleozoic arc and Triassic sedimentary rocks in the Yukon- Tanana terrane of northern British Columbia and southern Yukon, in Colpron, M., and Nelson, J.L., eds., Paleozoic Evolution and Metallogeny of Pericratonic Terranes at the Ancient Pacific Margin of North America, Canadian and Alaskan Cordillera: Geological Association of Canada, Special Paper 45, p. 153–177.

Rubatto, D., 2002, Zircon trace element geochemistry: partitioning with garnet and the link between U–Pb ages and metamorphism: Chemical Geology, v. 184, p. 123–138, http://dx.doi.org/10.1016/S0009-2541(01)00355-2.

Rubatto, D., and Hermann, J., 2007, Zircon behaviour in deeply subducted rocks: Elements, v. 3, p. 31–35, http://dx.doi.org/10.2113/gselements.3.1.31.

Shirahata, K., and Hirajima, T., 1995, Chemically sector-zoned garnet in Sanbagawa schists: its mode of occurrence and growth timing: Journal of Mineralogy, Petrology and Economic Geology, v. 90, p. 69–79, http://dx.doi.org/10.2465/ganko.90.69.

Simard, R.-L., Dostal, J., and Roots, C.F., 2003, Development of late Paleozoic volcanic arcs in the Canadian Cordillera: an example from the Klinkit Group, northern British Columbia and southern Yukon: Canadian Journal of Earth Sciences, v. 40, p. 907–924, http://dx.doi.org/10.1139/e03-025.

Smith, D.C., 1984, Coesite in clinopyroxene in the Caledonides and its implications for geodynamics: Nature, v. 310, p. 641–644, http://dx.doi.org/10.1038/310641a0.

Stacey, J.S., and Kramers, J.D., 1975, Approximation of terrestrial lead isotope evolution by a two-stage model: Earth and Planetary Science Letters, v. 26, p. 207–221, http://dx.doi.org/10.1016/0012-821X(75)90088-6.

Staples, R.D., Gibson, H.D., Berman, R.G., Ryan, J.J., and Colpron, M., 2013, A window into the Early to mid-Cretaceous infrastructure of the Yukon-Tanana terrane recorded in multi-stage garnet of west-central Yukon, Canada: Journal of Metamorphic Geology, v. 31, p. 729–753, http://dx.doi.org/10.1111/jmg.12042.

Stipp, M., Stünitz, H., Heilbronner, R., and Schmid, S.M., 2002, The eastern Tonale fault zone: a 'natural laboratory' for crystal plastic deformation of quartz over a temperature range from 250 to 700°C: Journal of Structural Geology, v. 24, p. 1861–1884, http://dx.doi.org/10.1016/S0191-8141(02)00035-4.

Sun, S.–s., and McDonough, W.F., 1989, Chemical and isotopic systematics of oceanic basalts: implications for mantle composition and processes: Geological Society, London, Special Publications, v. 42, p. 313–345, http://dx.doi.org/10.1144/GSL.SP.1989.042.01.19.

Tempelman-Kluit, D.J., 1977, Geology of Quiet Lake and Finlayson Lake map areas, Yukon Territory: Geological Survey of Canada, Open File 486, 3 maps, scale: 1: 250,000, http://dx.doi.org/10.4095/129286.

Tempelman-Kluit, D.J., 1979, Transported cataclasite, ophiolite and granodiorite in the Yukon: evidence of arc-continent collision: Geological Survey of Canada, Paper, 79-14, 27 p., http://dx.doi.org/10.4095/105928.

Tempelman-Kluit, D.J., 2012, Geology of Quiet Lake and Finlayson Lake map areas, south-central Yukon – An early interpretation of bedrock stratigraphy and structure: Geological Survey of Canada, Open File 5487, 103 p., http://dx.doi.org/10.4095/291931.

Wain, A., 1997, New evidence for coesite in eclogite and gneisses: Defining an ultra-high-pressure province in the Western Gneiss Region of Norway: Geology, v. 25, p. 927–930, http://dx.doi.org/10.1130/0091-7613(1997)025<0927:NEFCIE>2.3.CO;2.

Wang, X., and Liou, J.G., 1991, Regional ultrahigh-pressure coesite-bearing eclogitic terrane in central China: Evidence from country rocks, gneiss, marble, and metapelite: Geology, v. 19, p. 933–936, http://dx.doi.org/10.1130/0091-7613(1991)019<0933:RUPCBE>2.3.CO;2.

Wheeler, J.O., and McFeely, P., 1991, Tectonic map of the Canadian Cordillera and adjacent parts of the USA: Geological Society of Canada, "A" Series Map 1712A, scale: 1:2,000,000, http://dx.doi.org/10.4095/133549.

Wheeler, J.O., Brookfield, A.J., Gabrielse, H., Monger, J.W.H., Tipper, H.W., and Woodsworth, G.J., 1991, Terrane map of the Canadian Cordillera: Geological Survey of Canada, "A" Series Map 1713A, scale: 1:2,000,000, http://dx.doi.org/10.4095/133550.

Whitney, D.L., and Evans, B.W., 2010, Abbreviations for names of rock-forming minerals: American Mineralogist, v. 95, p. 185–187, http://dx.doi.org/10.2138/am.2010.3371.

Williams, I.S., 1998, U–Th–Pb geochronology by ion microprobe, *in* McKibben, M.A., Shanks III, W.C., and Ridley, W.I., *eds.*, Applications of microanalytical techniques to understand mineralizing processes: Reviews in Economic Geology, v. 7, p. 1–35.

Zhang, R.Y., Hirajima, T., Banno, S., Cong, B., and Liou, J.G., 1995, Petrology of ultrahigh-pressure rocks from the southern Su-Lu region, eastern China: Journal of Metamorphic Geology, v. 13, p. 659–675, http://dx.doi.org/10.1111/j.1525-1314.1995.tb00250.x.

For access to Petrie et al. (2015) electronic supplementary materials (Tables DR-1 through -8), please visit GAC's open source GC Data Repository, the Andrew Hynes Series: Tectonic Processes link at http://www.gac.ca/wp/?page_id=306.